

CVAP-TR-78-010
MAY 1978

CODE VERIFICATION AND APPLICATIONS PROGRAM

EMPIRICALLY BASED MODELING
TECHNIQUES FOR PREDICTING CRITICAL
FLOW RATES IN NOZZLES, TUBES, AND ORIFICES

by
D. G. Hall

NRC Research and Technical
Assistance Report



EG&G Idaho, Inc.



IDAHO NATIONAL ENGINEERING LABORATORY

DEPARTMENT OF ENERGY

IDAHO OPERATIONS OFFICE UNDER CONTRACT EY-76-C-07-1570

7812270348

NOTICE

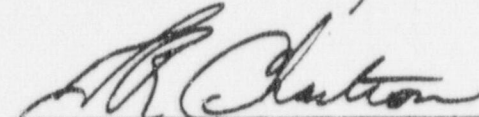
This report was prepared as an account of work sponsored by the United States Government. Neither the United States nor the Department of Energy, nor the Nuclear Regulatory Commission, nor any of their employees, nor any of their contractors, subcontractors, or their employees, makes any warranty, express or implied, or assumes any legal liability or responsibility for the accuracy, completeness or usefulness of any information, apparatus, product or process disclosed, or represents that its use would not infringe privately owned rights.

EMPIRICALLY BASED MODELING
TECHNIQUES FOR PREDICTING CRITICAL
FLOW RATES IN NOZZLES, TUBES, AND ORIFICES

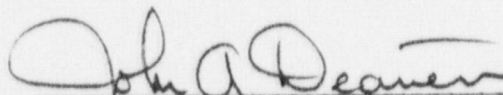
by
D. G. Hall

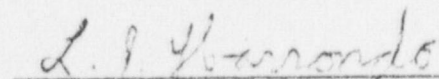
REVIEWED BY:


T. D. Knight, Section Leader


T. R. Charlton, Branch Manager

APPROVED BY:


J. A. Dearien, Manager
Code Verification and
Applications Program


L. J. Ybarrondo, Director
Water Reactor Research

This document has not received patent clearance and is
not to be released to the public domain.

EMPIRICALLY BASED MODELING
TECHNIQUES FOR PREDICTING CRITICAL
FLOW RATES IN NOZZLES, TUBES, AND ORIFICES

By

Douglas G. Hall

EG&G IDAHO, INC.

May 1978

PREPARED FOR THE
U.S. NUCLEAR REGULATORY COMMISSION
AND
DEPARTMENT OF ENERGY
IDAHO OPERATIONS OFFICE
UNDER CONTRACT NO. EY-76-C-07-1570

ACKNOWLEDGMENTS

The author wishes to express his thanks to D. L. Terry for excellent support in performing computer related tasks and for general management of the large volume of information that was produced during the course of the study; to L. M. Tomasko for help in obtaining the final computer-generated plots; to D. M. Snider for producing several of the FORTRAN subroutines used in making the calculations; to S. E. Jennings, S. A. Wilson, and members of the Word Processing Branch for typing the various drafts of the report; to members of the Reports and Service Division for their graphics and editorial support; and to T. D. Knight, R. E. Rice and O. J. Demuth for their helpful comments stemming from their reviews of the rough draft.

ABSTRACT

The objective of this study was to compare four critical flow models and a Bernoulli mass flux expression to separate effects critical flow data from Semiscale and the General Electric Company. Critical flow multipliers were determined empirically from the comparisons. The sensitivities of the critical flow multipliers to fluid stagnation conditions and flow duct geometry were also investigated. The root-mean-square deviation of the calculated critical flow from the data is presented.

SUMMARY

The objective of the study was to compare four critical flow models and a Bernoulli mass flux expression to separate effects critical flow data from Semiscale and the General Electric Company. The critical flow models were the HEM (homogeneous equilibrium model), the Henry-Fauske model, the Modified Burnell model, and the Bernoulli/HEM. The data comparisons permitted the empirical determination of critical flow multipliers for each model and root-mean-square deviations, or accuracies, of the model from the data. The sensitivities of the critical flow multipliers to fluid stagnation conditions and flow duct geometry were investigated.

The flow ducts from which the data were obtained included the following:

1. Converging-diverging nozzles with throat diameters from 0.43 to 2.45 centimeters.
2. Tubes with a 1.27 centimeter diameter, from 0 to 63.5 centimeters long.
3. An orifice with a 1.27 centimeter diameter.

The fluid stagnation conditions varied from 3000 to 13000 kPa and from 70 K subcooled to 50% quality.

Several significant conclusions were drawn from the results of the study. The Bernoulli/HEM model with appropriate multipliers produced the best predictions of critical flow rates in nozzles and orifices.

The Henry-Fauske model with associated multipliers demonstrated the most consistent accuracy in predicting critical flow rates in tubes for subcooled and low quality (less than 2%) saturated stagnation conditions; however, the multiplier values applicable to the subcooled and low quality regimes differed significantly. The HEM with an associated multiplier best predicted critical flow rates in a tube at higher stagnation qualities. These models in general produced critical flow rates within $\pm 10\%$ of the measured values.

The results of the study indicated that of the models currently available in RELAP4, the Henry-Fauske/HEM combination critical flow model is the most generally applicable. This conclusion is based on the individual performance of the Henry-Fauske model for subcooled stagnation conditions and the HEM for saturated stagnation conditions with qualities greater than 2%. The performance of the combination models Henry-Fauske/HEM and Modified Burnell/HEM was not assessed for transition qualities from 0 to 2%. The performance at transition conditions has a significant effect on the selection of a critical flow model for cases in which transition qualities exist for extended periods. Computational accuracies better than those exhibited by the Henry-Fauske/HEM may be achieved by using the information presented in this report to select an appropriate critical flow model for a specific flow situation.

NOMENCLATURE

| <u>Symbol</u> | <u>Description</u> | <u>Typical Units</u> |
|---------------|--|--------------------------------|
| A | Area or upstream area | cm^2 |
| C | Critical flow multiplier | |
| CN1 | Semiscale nozzle throat static pressure, tap number one | kPa |
| CN2 | Semiscale nozzle throat static pressure, tap number two | kPa |
| CN3 | Semiscale nozzle throat static pressure, tap number three | kPa |
| CN4 | Semiscale nozzle throat static pressure, tap number four | kPa |
| FDB | Semiscale broken loop drag disk measurement | $\text{kg/m} \cdot \text{s}^2$ |
| FTB | Semiscale broken loop turbine flowmeter measurement | m^3/s |
| G | Mass flux | $\text{kg/s} \cdot \text{m}^2$ |
| GB | Semiscale broken loop density | kg/m^3 |
| PB | Semiscale broken loop pressure | kPa |
| RMS | Root-mean-square | |
| SUB | Subcooled | |
| SAT | Saturated | |
| TFB | Semiscale broken loop temperature | K |
| VR | Vertical | |
| α | Void fraction | |

| | | |
|---|--|--------------------|
| d | Diameter | cm |
| ℓ | Length | cm |
| m | Mass | kg |
| p | Pressure | kPa |
| t | Time after rupture | s |
| w | Mass flow rate | kg/s |
| v | specific volume | m ³ /kg |
| x | Mass quality (mass of vapor/mass of mixture), or universal quality $[(v-v_g(p))/(v_v(p) - v_g(p))]$. These definitions are consistent for $0 \leq x \leq 1.0$. | |
| β | Orifice diameter ratio, d_{orif}/d_{pipe} | |
| δ | Percent deviation, $100(w_m - w_c')/w_c'$ | |
| ρ | Density | kg/m ³ |
| σ | Root-mean-square deviation | |

| <u>Superscripts</u> | <u>Description</u> |
|---------------------|---|
| ' | Value calculated using a critical flow multiplier |
| * | Critical value or choked condition |

| <u>Subscripts</u> | <u>Description</u> |
|-------------------|---|
| Ber | Bernoulli |
| c | Calculated |
| E | Exit, conditions near the exit of the tubular flow passages |
| HEM | Homogeneous equilibrium model |

| | |
|---------|--|
| ℓ | Saturated liquid |
| m | Measured |
| o | Stagnation |
| orif | Orifice |
| pipe | Pipe |
| th or T | Condition at the throat, minimum area point, or tube exit |
| trans | Transition |
| v | Saturated vapor |

CONTENTS

| | |
|--|-----|
| ACKNOWLEDGMENTS | ii |
| ABSTRACT. | iii |
| SUMMARY | iv |
| NOMENCLATURE. | vi |
| I. INTRODUCTION | 1 |
| II. INVESTIGATIVE APPROACH | 5 |
| 1. CRITICAL FLOW PARAMETER CALCULATIONS. | 5 |
| 2. STATISTICAL ANALYSES. | 8 |
| III. DATA BASE DESCRIPTION. | 12 |
| 1. SEMISCALE EXPERIMENTS | 12 |
| 2. GENERAL ELECTRIC EXPERIMENTS. | 19 |
| IV. DISCUSSION OF RESULTS. | 23 |
| 1. BASIC CRITICAL FLOW CALCULATION CONSIDERATIONS. | 24 |
| 2. THE EFFECT OF STAGNATION QUALITY RANGE. | 36 |
| 3. THE EFFECT OF FLOW PASSAGE GEOMETRIC PARAMETERS | 42 |
| V. CONCLUSIONS AND RECOMMENDATIONS. | 63 |
| VI. REFERENCES | 67 |
| APPENDIX A - BASIC INPUT AND OUTPUT DATA. | 70 |
| 1. SEMISCALE EXPERIMENTS | 77 |
| 1.1 Semiscale Test S-05-6. | 78 |
| 1.2 Semiscale Test S-02-4. | 89 |
| 1.3 Semiscale Test S-29-1. | 101 |
| 1.4 Semiscale Test S-02-6. | 111 |
| 1.5 Semiscale Test S-06-5. | 121 |
| 2. GENERAL ELECTRIC EXPERIMENTS. | 133 |
| 2.1 Nozzle 1 | 133 |
| 2.2 Nozzle 2 | 144 |

| | | |
|---|--|-----|
| 2.3 | Nozzle 3 | 187 |
| 3. | REFERENCES. | 198 |
| APPENDIX B - THE EFFECT OF STAGNATION QUALITY RANGE ON CRITICAL | | |
| | FLOW MULTIPLIER VALUE AND CALCULATIONAL ACCURACY . . . | 199 |
| 1. | NOZZLE FLOW PASSAGES. | 202 |
| 1.1 | Semiscale Test S-05-6. | 203 |
| 1.2 | Semiscale Test S-02-4. | 209 |
| 1.3 | Semiscale Test S-29-1. | 214 |
| 1.4 | GE Nozzle 1. | 218 |
| 1.5 | Semiscale Test S-02-6. | 224 |
| 2. | TUBULAR FLOW PASSAGES | 229 |
| 2.1 | GE Nozzle 2, $l/d = 0$ | 230 |
| 2.2 | Semiscale Test S-06-5 ($l/d = 4$). | 234 |
| 2.3 | GE Nozzle 2, $l/d = 9$ | 238 |
| 2.4 | GE Nozzle 2, $l/d = 18$ | 245 |
| 2.5 | GE Nozzle 2, $l/d = 50$ | 245 |
| 3. | REFERENCES. | 253 |

FIGURES

| | | |
|-----|--|----|
| 1. | Plan view of Semiscale vessel side broken cold-leg piping with associated instrumentation. | 13 |
| 2. | Semiscale Pipe Spool 23 and interchangeable nozzle insert . . . | 14 |
| 3. | Semiscale nozzle break simulator configurations | 15 |
| 4. | Semiscale tubular break simulator configuration | 16 |
| 5. | Schematic of General Electric critical flow test equipment. . . | 20 |
| 6. | General Electric critical flow test duct configurations | 21 |
| 7. | Effect of nozzle diameter ratio on subcooled regime critical flow multipliers. | 45 |
| 8. | Effect of nozzle diameter ratio on subcooled regime RMS percent deviations. | 47 |
| 9. | Effect of nozzle diameter ratio on transition regime critical flow multipliers. | 49 |
| 10. | Effect of nozzle diameter ratio on transition regime RMS percent deviations. | 50 |
| 11. | Effect of nozzle diameter ratio on saturated regime critical flow multipliers. | 52 |
| 12. | Effect of nozzle diameter ratio on saturated regime RMS percent deviations. | 53 |
| 13. | Effect of tubular length-to-diameter ratio on subcooled regime critical flow multipliers. | 55 |
| 14. | Effect of tubular length-to-diameter ratio on subcooled regime RMS percent deviations | 58 |
| 15. | Effect of tubular length-to-diameter ratio on transition regime critical flow multipliers. | 59 |
| 16. | Effect of tubular length-to-diameter ratio on transition regime RMS percent deviations | 61 |

| | | |
|-------|---|----|
| A-1. | Semiscale nozzle break simulator configurations. | 72 |
| A-2. | Semiscale Pipe Spool 23 and interchangeable nozzle insert | 73 |
| A-3. | Semiscale tubular break simulator configuration. | 74 |
| A-4. | General Electric critical flow test duct configurations. . | 75 |
| A-5. | Schematic of General Electric critical flow test equip- ment | 76 |
| A-6. | Stagnation pressure history (Semiscale Test S-05-6). | 79 |
| A-7. | Stagnation temperature history (Semiscale Test S-05-6) | 80 |
| A-8. | Stagnation density history (Semiscale Test S-05-6). | 81 |
| A-9. | Stagnation quality history (Semiscale Test S-05-6). | 82 |
| A-10. | Comparison of measured throat pressures and calculated critical pressures (Semiscale Test S-05-6). | 84 |
| A-11. | Comparison of measured throat pressure ratios and calculated critical pressure ratios (Semiscale Test S-05-6) | 85 |
| A-12. | Comparison of measured mass flow rates and calculated critical flow rates (Semiscale Test S-05-6). | 86 |
| A-13. | Ratios of measured-to-calculated mass flow rates (Semiscale Test S-05-6) | 87 |
| A-14. | Stagnation pressure history (Semiscale Test S-02-4) | 91 |
| A-15. | Stagnation temperature history (Semiscale Test S-02-4) | 92 |
| A-16. | Stagnation density history (Semiscale Test S-02-4) | 93 |
| A-17. | Stagnation quality history (Semiscale Test S-02-4) | 94 |
| A-18. | Comparison of measured throat pressures and calculated critical pressures (Semiscale Test S-02-4). | 95 |

| | | |
|-------|---|-----|
| A-19. | Comparison of measured throat pressure ratios and calculated critical pressure ratios (Semiscale Test S-02-4) | 96 |
| A-20. | Comparison of measured break flow rate and calculated critical flow rate (Semiscale Test S-02-4). | 98 |
| A-21. | Ratios of measured-to-calculated break flow rates (Semiscale Test S-02-4) | 99 |
| A-22. | Stagnation pressure history (Semiscale Test S-29-1) | 102 |
| A-23. | Stagnation temperature history (Semiscale Test S-29-1) | 103 |
| A-24. | Stagnation density history (Semiscale Test S-29-1) | 104 |
| A-25. | Stagnation quality history (Semiscale Test S-29-1) | 105 |
| A-26. | Comparison of calculated critical pressures (Semiscale Test S-29-1). | 106 |
| A-27. | Comparison of calculated critical pressure ratios (Semiscale Test S-29-1) | 107 |
| A-28. | Comparison of measured break flow rates and calculated critical flow rates (Semiscale Test S-29-1) | 108 |
| A-29. | Ratios of measured-to-calculated mass flow rates (Semiscale Test S-29-1). | 109 |
| A-30. | Stagnation pressure history (Semiscale Test S-02-6) | 112 |
| A-31. | Stagnation temperature history (Semiscale Test S-02-6) | 113 |
| A-32. | Stagnation density history (Semiscale Test S-02-6) | 114 |
| A-33. | Stagnation quality history (Semiscale Test S-02-6) | 115 |
| A-34. | Comparison of calculated critical pressures (Semiscale Test S-02-6). | 116 |
| A-35. | Comparison of calculated critical pressure ratios (Semiscale Test S-02-6) | 117 |

| | | |
|-------|---|-----|
| A-36. | Comparison of measured break flow rates and calculated critical flow rates (Semiscale Test S-02-6) | 119 |
| A-37. | Ratios of measured-to-calculated break flow rates (Semiscale Test S-02-6) | 120 |
| A-38. | Stagnation pressure history (Semiscale Test S-06-5) | 123 |
| A-39. | Stagnation temperature history (Semiscale Test S-06-5) | 124 |
| A-40. | Stagnation density history (Semiscale Test S-06-5) | 125 |
| A-41. | Stagnation quality history (Semiscale Test S-06-5) | 126 |
| A-42. | Comparison of measured throat pressures and calculated critical pressures (Semiscale Test S-06-5). | 127 |
| A-43. | Comparison of measured throat pressure ratios and calculated critical pressure ratios (Semiscale Test S-06-5) | 128 |
| A-44. | Comparison of measured break flow rates and calculated critical flow rates (Semiscale Test S-06-5). | 131 |
| A-45. | Ratios of measured-to-calculated break flow rates (Semiscale Test S-06-5) | 132 |
| A-46. | Stagnation pressure data (GE Nozzle 1) | 135 |
| A-47. | Stagnation temperature data (GE Nozzle 1). | 136 |
| A-48. | Stagnation density data (GE Nozzle 1). | 137 |
| A-49. | Comparison of measured throat pressures and calculated HEM critical pressures (GE Nozzle 1). | 138 |
| A-50. | Comparison of measured throat pressure ratios and calculated critical pressure ratios (GE Nozzle 1). | 139 |
| A-51. | Comparison of measured mass fluxes and HEM critical mass fluxes (GE Nozzle 1) | 141 |
| A-52. | Ratios of measured-to-calculated mass fluxes (GE Nozzle 1). | 143 |

| | | |
|-------|--|-----|
| A-53. | Stagnation pressure data (GE Nozzle 2, $l/d = 0$) | 146 |
| A-54. | Stagnation temperature data (GE Nozzle 2, $l/d = 0$) | 147 |
| A-55. | Stagnation density data (GE Nozzle 2, $l/d = 0$) | 148 |
| A-56. | Comparison of measured exit pressures and calculated critical pressures (GE Nozzle 2, $l/d = 0$) | 149 |
| A-57. | Comparison of measured exit pressure ratios and calculated critical pressure ratios (GE Nozzle 2, $l/d = 0$) | 150 |
| A-58. | Comparison of measured mass fluxes and calculated critical mass fluxes (GE Nozzle 2, $l/d = 0$) | 151 |
| A-59. | Ratios of measured to calculated mass fluxes (GE Nozzle 2, $l/d = 0$) | 152 |
| A-60. | Stagnation pressure data (GE Nozzle 2, $l/d = 9$) | 153 |
| A-61. | Stagnation temperature data (GE Nozzle 2, $l/d = 9$) | 154 |
| A-62. | Stagnation density data (GE Nozzle 2, $l/d = 9$) | 155 |
| A-63. | Comparison of calculated critical pressures (GE Nozzle 2, $l/d = 9$) | 157 |
| A-64. | Comparison of calculated critical pressure ratios (GE Nozzle 2, $l/d = 9$) | 158 |
| A-65. | Comparison of measured mass fluxes and calculated critical mass fluxes (GE Nozzle 2, $l/d = 9$) | 159 |
| A-66. | Ratios of measured-to-calculated mass fluxes (GE Nozzle 2, $l/d = 9$) | 160 |
| A-67. | Stagnation pressure data (GE Nozzle 2, $l/d = 18$) | 161 |
| A-68. | Stagnation temperature data (GE Nozzle 2, $l/d = 18$) | 162 |
| A-69. | Stagnation density data (GE Nozzle 2, $l/d = 18$) | 163 |
| A-70. | Comparison of measured exit pressures and calculated critical pressures (GE Nozzle 2, $l/d = 18$) | 164 |
| A-71. | Comparison of measured exit pressure ratios and calculated critical pressure ratios (GE Nozzle 2, $l/d = 18$) | 165 |
| A-72. | Comparison of measured mass fluxes and calculated critical mass fluxes (GE Nozzle 2, $l/d = 18$) | 166 |

| | | |
|-------|--|-----|
| A-73. | Ratios of measured-to-calculated mass fluxes (GE Nozzle 2, $\ell/d = 18$). | 167 |
| A-74. | Stagnation pressure data (GE Nozzle 2, $\ell/d = 50$) | 168 |
| A-75. | Stagnation temperature data (GE Nozzle 2, $\ell/d = 50$). | 169 |
| A-76. | Stagnation density data (GE Nozzle 2, $\ell/d = 50$). | 170 |
| A-77. | Comparison of measured exit pressures and calculated critical pressures (GE Nozzle 2, $\ell/d = 50$). | 171 |
| A-78. | Comparison of measured exit pressure ratios and calculated critical pressure ratios (GE Nozzle 2, $\ell/d = 50$). | 172 |
| A-79. | Comparison of measured mass fluxes and calculated critical mass fluxes (GE Nozzle 2, $\ell/d = 50$) | 173 |
| A-80. | Ratios of measured-to-calculated mass fluxes (GE Nozzle 2, $\ell/d = 50$). | 174 |
| A-81. | The effect of flow path geometry on critical mass flux | 178 |
| A-82. | Ratios of measured break flow rates to HEM calculated critical flow rates (Semiscale Test S-02-4). | 185 |
| A-83. | Stagnation pressure data (GE Nozzle 3) | 189 |
| A-84. | Stagnation temperature data (GE Nozzle 3). | 190 |
| A-85. | Stagnation density data (GE Nozzle 3). | 191 |
| A-86. | Comparison of measured orifice pressures and calculated critical pressures (GE Nozzle 3). | 192 |
| A-87. | Comparison of measured orifice pressure ratios and calculated critical pressure ratios (GE Nozzle 3) | 193 |
| A-88. | Comparisons of measured mass fluxes and calculated critical mass fluxes (GE Nozzle 3). | 194 |
| A-89. | Ratios of measured-to-calculated mass fluxes (GE Nozzle 3). | 195 |

| | | |
|-------|---|-----|
| B-1. | Bernoulli/HEM mass flow ratio as a function of stagnation universal quality (Semiscale Test S-05-6) | 204 |
| B-2. | Bernoulli/HEM critical flow multiplier as a function of stagnation quality range limit (Semiscale Test S-05-6). | 206 |
| B-3. | Bernoulli/HEM RMS percent deviation as a function of stagnation quality range limit (Semiscale Test S-05-6). | 208 |
| B-4. | Bernoulli/HEM mass flow ratio as a function of stagnation universal quality (Semiscale Test S-02-4) | 210 |
| B-5. | Bernoulli/HEM critical flow multiplier as a function of stagnation quality range limit (Semiscale Test S-02-4). | 211 |
| B-6. | Bernoulli/HEM RMS percent deviation as a function of stagnation quality range limit (Semiscale Test S-02-4). | 213 |
| B-7. | Bernoulli/HEM mass flow ratio as a function of stagnation universal quality (Semiscale Test S-29-1). | 215 |
| B-8. | Bernoulli/HEM critical flow multiplier as a function of stagnation quality range limit (Semiscale Test S-29-1). | 217 |
| B-9. | Bernoulli/HEM RMS percent deviation as a function of stagnation quality range limit (Semiscale Test S-29-1). | 219 |
| B-10. | Bernoulli/HEM mass flow ratio as a function of stagnation universal quality (GE Nozzle 1). | 220 |
| B-11. | Bernoulli/HEM critical flow multiplier as a function of stagnation quality range limit (GE Nozzle 1). | 222 |
| B-12. | Bernoulli/HEM RMS percent deviation as a function of stagnation quality range limit (GE Nozzle 1). | 223 |
| B-13. | Bernoulli/HEM mass flow ratio as a function of stagnation universal quality (Semiscale Test S-02-6) | 225 |
| B-14. | Bernoulli/HEM critical flow multiplier as a function of stagnation quality range limit (Semiscale Test S-02-6). | 226 |

| | | |
|-------|---|-----|
| B-15. | Bernoulli/HEM RMS percent deviation as a function of stagnation quality range limit (Semiscale Test S-02-6). | 227 |
| B-16. | Henry-Fauske mass flow ratio as a function of stagnation universal quality (GE Nozzle 2, $l/d = 0$) | 231 |
| B-17. | Henry-Fauske critical flow multiplier as a function of stagnation quality range limit (GE Nozzle 2, $l/d = 0$) | 232 |
| B-18. | Henry-Fauske RMS percent deviation as a function of stagnation quality range limit (GE Nozzle 2, $l/d = 0$) | 233 |
| B-19. | Henry-Fauske mass flow ratio as a function of stagnation universal quality (Semiscale Test S-06-5) | 235 |
| B-20. | Henry-Fauske critical flow multiplier as a function of stagnation quality range limit (Semiscale Test S-06-5). | 236 |
| B-21. | Henry-Fauske RMS percent deviation as a function of stagnation quality range limit (Semiscale Test S-06-5). | 237 |
| B-22. | HEM mass flow ratio as a function of stagnation universal quality (Semiscale Test S-06-5). | 239 |
| B-23. | HEM critical flow multiplier as a function of stagnation quality range limit (Semiscale Test S-06-5) | 240 |
| B-24. | HEM RMS percent deviation as a function of stagnation quality range limit (Semiscale Test S-06-5). | 241 |
| B-25. | Henry-Fauske mass flow ratio as a function of stagnation universal quality (GE Nozzle 2, $l/d = 9$) | 242 |
| B-26. | Henry-Fauske critical flow multiplier as a function of stagnation quality range limit (GE Nozzle 2, $l/d = 9$) | 243 |
| B-27. | Henry-Fauske RMS percent deviation as a function of stagnation quality range limit (GE Nozzle 2, $l/d = 9$) | 244 |
| B-28. | Henry-Fauske mass flow ratio as a function of stagnation universal quality (GE Nozzle 2, $l/d = 18$). | 246 |

| | | |
|-------|---|-----|
| B-29. | Henry-Fauske critical flow multiplier as a function of stagnation quality range limit (GE Nozzle 2, $l/d = 18$). | 247 |
| B-30. | Henry-Fauske RMS percent deviation as a function of stagnation quality range limit (GE Nozzle 2, $l/d = 18$). | 248 |
| B-31. | Henry-Fauske mass flow ratio as a function of stagnation quality range limit (GE Nozzle 2, $l/d = 50$). | 249 |
| B-32. | Henry-Fauske critical flow multiplier as a function of stagnation quality range limit (GE Nozzle 2, $l/d = 50$). | 251 |
| B-33. | Henry-Fauske RMS percent deviation as a function of stagnation quality range limit (GE Nozzle 2, $l/d = 50$). | 252 |

TABLES

| | | |
|------|--|----|
| I. | Inventory of Data Points and Stagnation Fluid Property Ranges Obtained from Semiscale Tests | 18 |
| II. | Inventory of Data Points and Stagnation Fluid Property Ranges Obtained from General Electric Tests | 22 |
| III. | Critical Flow Multiplier and RMS Percent Deviation Data for Nozzles. | 25 |
| IV. | Critical Flow Multiplier and RMS Percent Deviation Data for Tubes. | 26 |
| V. | Critical Flow Multiplier and RMS Percent Deviation Data for an Orifice | 27 |
| VI. | Variation in Critical Flow Multipliers and RMS Percent Deviations. | 38 |

EMPIRICALLY BASED MODELING
TECHNIQUES FOR PREDICTING CRITICAL
FLOW RATES IN NOZZLES, TUBES, AND ORIFICES

I. INTRODUCTION

An analytical model of critical flow phenomena is required in the computer model of a water cooled reactor system. LOCA (loss of coolant accident) experiments have shown that core thermal response is quite sensitive to the break flow rates. Therefore, reactor safety analyses require accurate prediction of the break flow rates. The critical flow study reported in Reference 1 showed that break flow rates during a LOCA transient are dependent on fluid conditions and flow path geometry. Different critical flow models were required when the stagnation conditions were subcooled, saturated with little quality, or saturated with appreciable quality. Flow multipliers significantly different from unity can be required to obtain good agreement between measured and calculated break flow rates when choking occurs in a nozzle.

The RELAP4 computer code^[2] is used to calculate the response of a water cooled reactor system during a LOCA transient. Critical flow modeling permits a combination of two critical flow models to calculate break flow rates during the course of the transient. User selected critical flow multipliers may be input. A multiplier is associated with each critical flow model and is applied to all critical flow rates

calculated with that particular model. Transition from one model to the other occurs over a stagnation quality range from zero to a user specified upper bound, x_{o_trans} .

The purpose of this report was to take the first step in establishing an empirical basis for the selection of RELAP4 critical flow modeling options and to assess the accuracy of critical flow calculations. This effort is part of a procedure for determining critical flow modeling techniques applicable to a wide range of fluid conditions and to various flow passage geometries up to full scale. Because of the lack of large scale critical flow data, data from relatively small scale experiments (choked cross section diameters on the order of 1.3 centimeters), in which choking occurred in tubes, nozzles, and orifices, were assembled in a data base for this study. These types of flow passages are typical of break simulators in LOCA experiments and of postulated break configurations for a full scale reactor. The approach taken in this report was to determine critical flow multipliers for each model which would produce the best agreement between measured and calculated mass flow rates for each test. The fundamental capability of the critical flow models to predict simultaneously both the critical flow rate and the thermodynamic state at the choke point was not evaluated. A first level evaluation of the calculational accuracy of the critical flow models and their associated multipliers assessed the accuracy with which the measured critical flow rates in the data base could be predicted. This evaluation allowed identification of the model(s) best suited for modeling critical flow rates in each of the three types of flow passages.

The dependence of the critical flow multipliers and calculational accuracies on the range of the stagnation conditions was evaluated. The dependence of the critical flow multiplier and accuracy on geometric parameters was also determined. Information was thus made available to guide the selection of options necessary for predicting critical flow rates in a given flow situation.

The basic presentation of the results of the study are in the form of tables which present critical flow multipliers and calculational accuracies for each model for specific flow passages and ranges of stagnation qualities. These tables are supplemented by a set of plots which illustrate the variation in critical flow multipliers and calculational accuracies with variations in nondimensional geometric parameters. Another table summarizes the effect of stagnation quality range on multiplier and accuracy values.

Two appendices contain the basic data for determining the critical flow multipliers, calculational accuracies, and associated sensitivities. Direct comparisons between measured and calculated critical flow parameters are presented in Appendix A as either time histories or as

functions of stagnation universal quality, x_0 [a]. Fluid properties input to the critical flow calculations are also presented in Appendix A in the same format. The plots presented in Appendix B show the dependence of critical flow multiplier and calculational accuracy on the range of stagnation quality.

[a] Universal quality x is defined by the equation:

$$x = [v - v_l(p)] / [v_v(p) - v_l(p)]$$

where v is the specific volume of the mixture, p is the state point pressure, and the saturated liquid and vapor specific volumes (v_l and v_v , respectively) are defined by the state point pressure only.

II. INVESTIGATIVE APPROACH

The study reported in this document was undertaken in two phases. During the first phase, critical flow parameters were calculated using four critical flow models and the Bernoulli mass flux expression^[a] with input data taken from a variety of experiments. The ratios of measured-to-calculated mass flow rates generated during the first phase were used as input for statistical analyses in the second phase of the study. The approach taken in each phase is described in detail in the two subsections that follow.

1. CRITICAL FLOW PARAMETER CALCULATIONS

Critical flow parameters were calculated using the following analytical expressions:

- 1) Homogeneous equilibrium model (HEM)
- 2) Henry-Fauske model^[3]
- 3) Modified Burnell model^{[4] [5]}
- 4) Bernoulli/HEM model^[1]
- 5) Bernoulli mass flux expression with measured throat pressure input.

[a] The Bernoulli mass flux expression is an inverted form of the Bernoulli equation expressed as:

$$G = \sqrt{2\rho_0 p_0 (1 - p/p_0)},$$

where G is the mass flux, ρ_0 is the stagnation density, and p is the static pressure, and p_0 is the stagnation pressure.

The homogeneous equilibrium, Henry-Fauske, and Modified Burnell critical flow models were used in performing the study because they are three of the basic models which are used by the RELAP4^[2] code, either separately or in combination, to compute critical flow rates. The Bernoulli/HEM critical flow model was used in performing the study because this model produced critical pressures and flow rates in the best agreement with measured values, as reported in Reference 1. The Bernoulli mass flux expression was used in performing the study because this expression is used by the Henry-Fauske and Modified Burnell models when the stagnation conditions are subcooled and because it was found in the study reported in Reference 1 to produce mass flow rates having a constant ratio relationship with measured mass flow rates when measured critical pressures were used in the expression.

The assumptions used in the derivation of the first three critical flow models along with the principal equations for each are presented in Appendix B of Reference 1. The Bernoulli/HEM model is a combination critical flow model with which critical flow rates are calculated using the Bernoulli mass flux expression when the stagnation conditions are subcooled and the homogeneous equilibrium model when the stagnation quality is greater than a selected transition quality. The critical flow rate calculated for stagnation qualities between 0 and x_{o_trans} is obtained by interpolating between the values calculated by the two models at the same stagnation conditions. This interpolation is expressed by the formula:

$$w = C_{Ber} w_{Ber} - \frac{x_o}{x_{o_{trans}}} (C_{Ber} w_{Ber} - C_{HEM} w_{HEM}) \quad (1)$$

where w_{Ber} and w_{HEM} are the mass flow rates calculated using the Bernoulli and homogeneous equilibrium models, respectively; C_{Ber} and C_{HEM} are the critical flow multipliers associated with the Bernoulli and homogeneous equilibrium models, respectively; x_o is the stagnation quality; and $x_{o_{trans}}$ is the lowest stagnation quality at which mass flow rates are calculated using only the homogeneous equilibrium model. The critical pressure ratios used for computing critical flow rates using the Bernoulli model were derived from a curve fit of throat-to-total pressure ratio as a function of stagnation universal quality, x_o . This empirical relationship was derived from data generated using a Semiscale break nozzle as described in Reference 1.

The fifth method of calculating critical flow rates was to use the measured throat-to-total pressure ratio as input to the Bernoulli mass flux expression along with the measured stagnation properties. It should be noted that this method of calculation does not constitute a critical flow model since it does not provide a method of calculating the thermodynamic state at the critical point. Calculations using this method were made to evaluate the Bernoulli expression characterization of critical flow processes without having to account for possible errors in predicting the thermodynamic state at the critical point.

The calculations of critical flow parameters were made by using a special purpose computer program, MASFLO, in which the critical flow models are coded. This program, which is described in Appendix A of Reference 1, computes critical flow parameters for an input set of stagnation fluid properties. The calculations made for each stagnation condition are independent of those made at other conditions; although, output parameters may be temporarily related if input data are taken from stagnation state histories as in the case of the Semiscale data. Calculations made with a given set of input data are made using whichever critical flow model the user selects. Tabulated data are produced which include the input stagnation fluid properties, the calculated critical point fluid properties, measured and calculated critical flow rates, and for most cases, the measured throat pressure. The data listed in the printed output are also stored on magnetic tape. Plots comparing measured and calculated critical pressure, critical pressure ratio, and mass flow rate and a plot of the ratio of measured-to-calculated mass flow rate were produced using the data stored on magnetic tape as input to a computer plotting software package.

2. STATISTICAL ANALYSES

In the second phase of the study, critical flow multipliers for use in conjunction with each critical flow model to compute critical flow rates for a specified flow passage and range of stagnation conditions were determined. In addition to determining the value of the critical flow multipliers, the accuracy of calculating critical flow rates used to determine the multipliers was assessed. This type of calculation accuracy has been

termed "first level" accuracy since it is based upon the same data as was used in the determination of the critical flow multiplier values. An assessment of "second level" accuracy would require the use of data other than or in addition to the original data. In particular, the data base for determining "second level" accuracy would include data at larger scale. It is conceivable that the use of the expanded data base might introduce a significant bias type error in the critical flow multiplier that is as significant, if not more so, as the "first level" calculational accuracy discussed in this report. Similarly, the effect of error in the stagnation conditions that are input into the critical flow model, an important consideration in system calculations, is not addressed. Thus, the first level calculational accuracies which were determined in the study are probably best possible accuracies with regard to the prediction of critical flow rates occurring at fluid conditions and in flow passages other than those used in the determination of the critical flow multiplier values. The calculational accuracy values include both errors attributable to the analytical model and errors caused by random measurement inaccuracies since no adjustment of the calculational accuracy values was made using measurement accuracy information. Removal of the random measurement errors would probably result in improved calculational accuracy values.

The statistical calculations were performed using stagnation universal qualities (x_0) calculated from the stagnation fluid properties and corresponding ratios of measured-to-calculated critical mass flow rate. The basic determination of the critical flow multipliers and calculational accuracy information involved dividing the quality and mass flow ratio data for each flow geometry into three regimes: subcooled, saturated with stagnation

qualities less than 2%, and saturated with stagnation qualities greater than 2%. These quality regimes correspond to those which were described in Reference 1 and delineate conditions for which the critical flow processes were different. The mass flow ratios, w_m/w_c , corresponding to the qualities in each regime were averaged to produce critical flow multiplier values. The RMS deviation of the mass flow ratios from the corresponding critical flow multiplier was also calculated. The ratio of the RMS mass flow ratio deviation to the critical flow multiplier is mathematically equivalent to the RMS deviation of the measured critical flow rate from the value calculated using the critical flow multiplier expressed as a percentage of the calculated value [i.e. $\delta = (w_m - w_c')/w_c'$]. The latter form of the parameter represents the RMS of the percent errors obtained for a set of data points and therefore provided a quantitative measure of the calculational accuracy that was obtained using the critical flow multipliers. The RMS of the percent errors is referred to by the term "RMS percent error" throughout this report. This information was used to determine which critical flow model produced critical flow rates in the best agreement with the data for a given quality regime.

The previously described basic approach produced critical mass flow multipliers associated with each critical flow model that should be used when performing critical flow calculations for a particular flow geometry with stagnation conditions in each of the three quality regimes. A quantitative index (RMS percent deviation) of how well the critical flow rates calculated using each critical flow model agreed with corresponding measured values was also obtained for each of the three quality regimes. Although this approach allowed comparisons to be made among the models

for a given set of data, it was not well suited to making investigations of how the critical flow multiplier and the accuracy values changed as a function of some geometric characteristic of the flow passage. The reason the approach was not adequate was that the data corresponding to different flow geometries did not cover the same range of stagnation qualities. For example, the multiplier derived for one geometry may have been obtained using data having corresponding stagnation universal qualities ranging from -2% to zero, while for another geometry the subcooled stagnation universal qualities may have been -0.5% to zero. It was therefore necessary to calculate critical flow multipliers and calculational accuracy values using data spanning the same range of stagnation qualities. Such data was obtained in the course of calculating critical flow multipliers and corresponding calculational accuracies using data contained in progressively larger subsets of all of the available data which was used in the first determination of the multiplier and accuracy values. The dependence of the multiplier and accuracy values on the range of the stagnation qualities corresponding to the data used in their determination was thus defined and allowed comparable values of these parameters to be obtained. The dependence of the critical flow multiplier and accuracy values on geometric parameters could then be properly determined.

III. DATA BASE DESCRIPTION

The data used to perform this study was obtained from five Semiscale LOCA experiments [6 through 10] and experiments conducted by the General Electric Company [11]. Descriptions of the systems used to perform the Semiscale and GE experiments are contained respectively in the two subsections that follow. Also included in these subsections are descriptions of the test flow passage geometries in which critical flow occurred and a tabulation of the fluid conditions at which each flow passage geometry was tested.

1. SEMISCALE EXPERIMENTS

The Semiscale data that were used in the study were measured during cold leg break LOCA experiments on the vessel side of the broken loop which is shown in Figure 1. This part of the system was used because of the simplicity of the flow path between the vessel and break simulator contained in Spool 23 and because of the redundancy of mass flow rate metering instrumentation. Spool 23 is designed to accept interchangeable break simulator inserts as shown in Figure 2. Each of the five experiments from which data were taken utilized a different insert. Four of the inserts contained converging-diverging nozzle flow passages of similar design, but varying throat diameter. The key dimensions of these configurations are presented in Figure 3. The remaining insert contained a tubular flow passage with a 10-degree half-angle, conical entrance section. The dimensions of this configuration are presented in Figure 4.

PB - Pressure
 FDB - Flow (drag disk)
 FTB - Flow (turbine flowmeter)
 TFB - Fluid Temperature
 GB - Density (vertical,

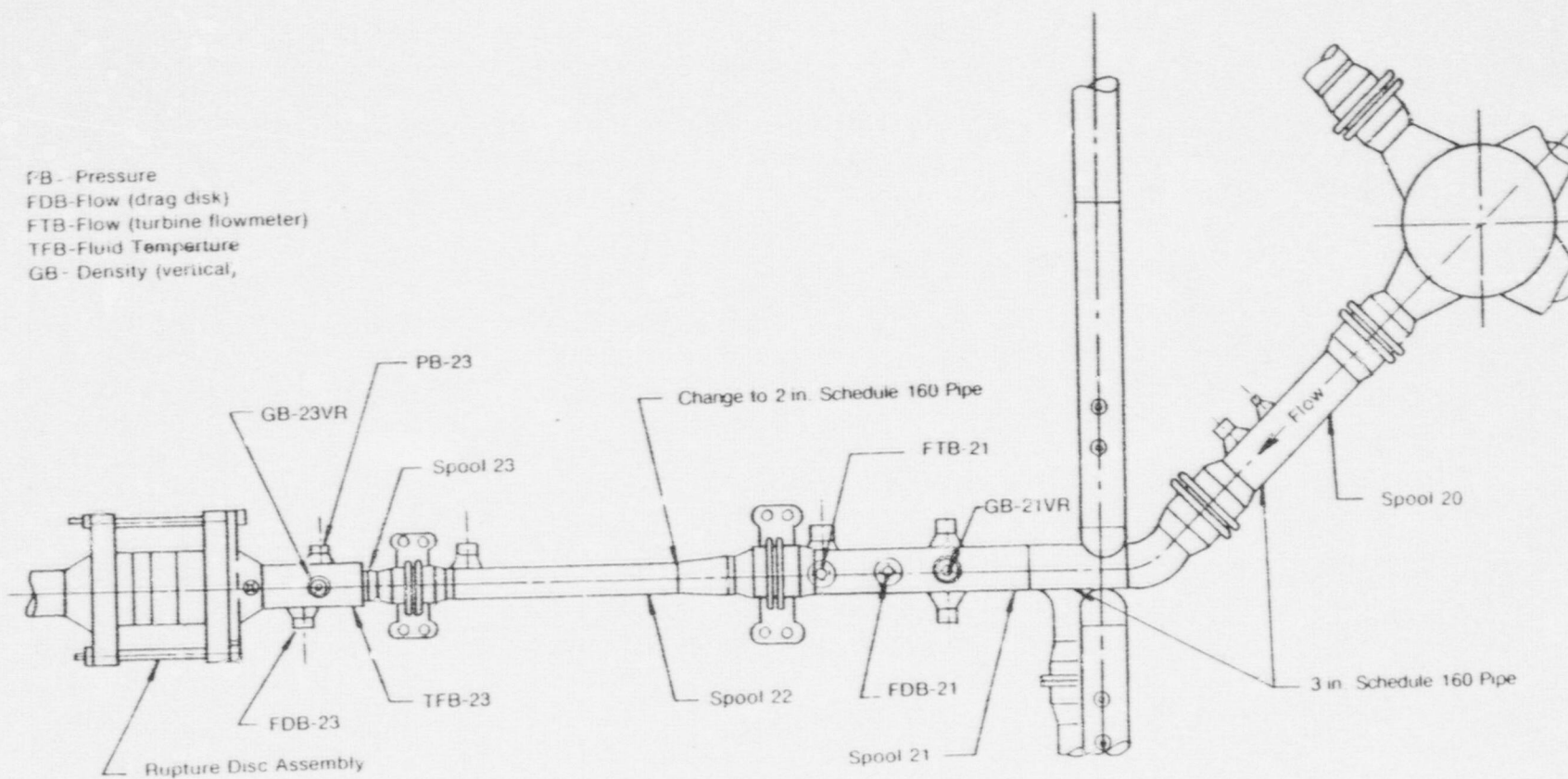


Fig. 1 Plan view of Semiscale vessel side broken cold-leg piping with associated instrumentation.

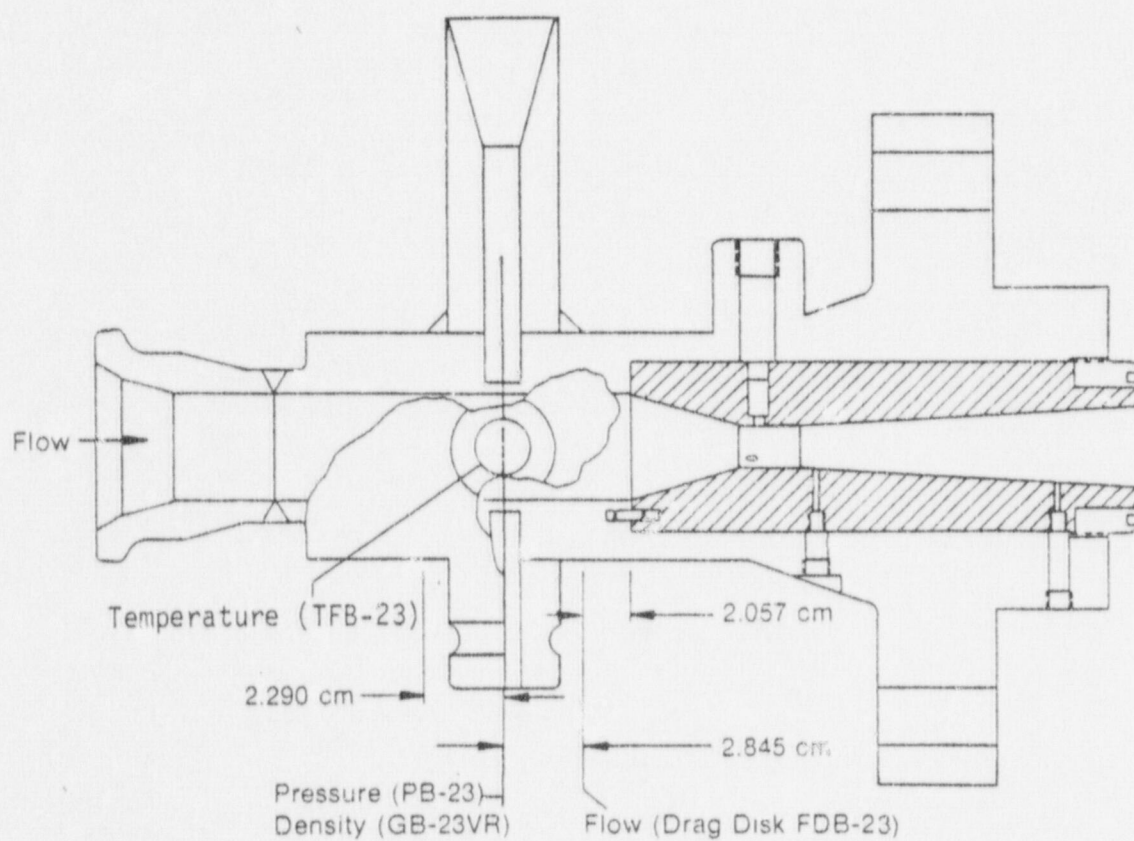
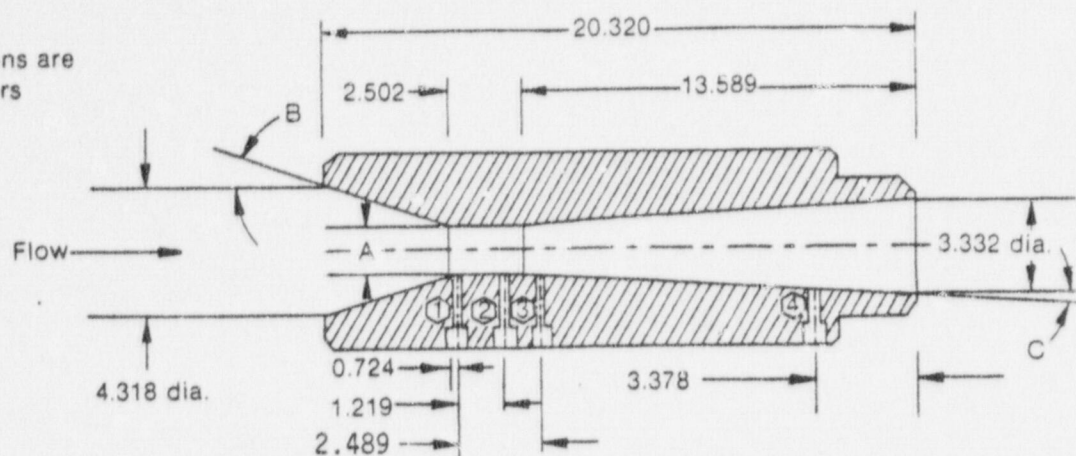
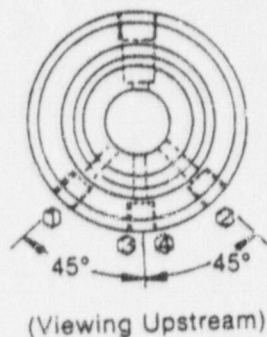


Fig. 2 Semiscale pipe spool 23 and interchangeable nozzle insert.

Note: All dimensions are in centimeters

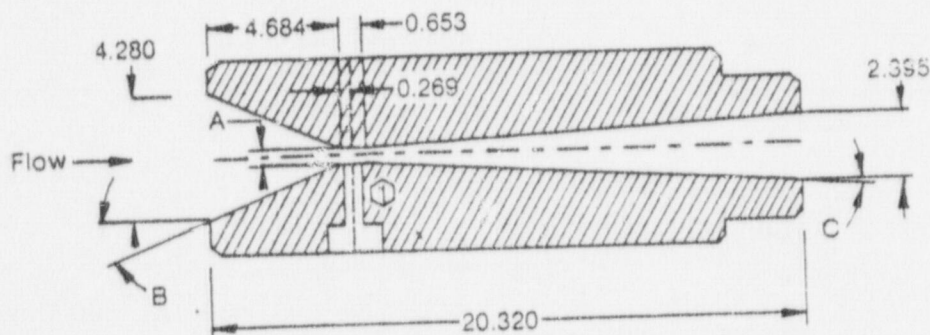


Pressure taps

- ① = PB-CN1
- ② = PB-CN2
- ③ = PB-CN3
- ④ = PB-CN4

| Test used for | Nozzle dia. ratio | A | B | C | Throat ℓ/d |
|---------------|-------------------|-------|---------|--------|-----------------|
| S-05-6 | 1.76 | 2.451 | 12° 25' | 1° 52' | 1.02 |
| S-02-4 | 2.45 | 1.760 | 16° 15' | 3° 19' | 1.42 |
| S-29-1 | 3.29 | 1.311 | 19° 34' | 4° 15' | 1.91 |

a. Larger throated nozzles

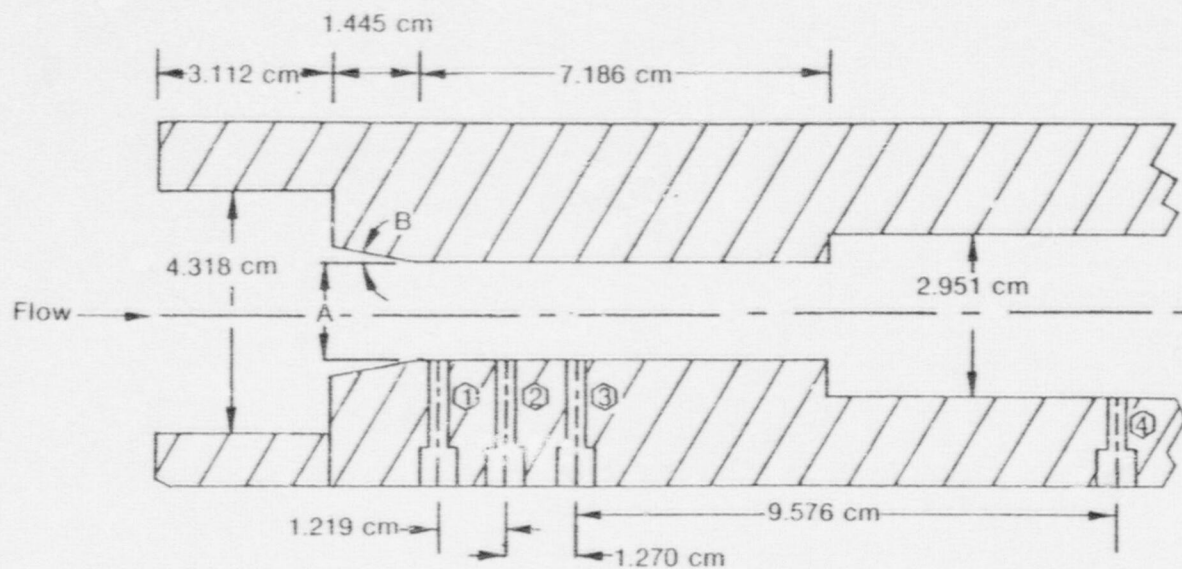


Pressure Tap
① = PB-CN1

| Test used for | A | B | C | Throat ℓ/d | Nozzle dia. ratio |
|---------------|-------|---------|--------|-----------------|-------------------|
| S-02-6 | 0.429 | 22° 21' | 3° 45' | 1.52 | 10.07 |

b. Small throated nozzle

Fig. 3 Semiscale nozzle break simulator configurations.



Pressure Taps

- ① = PB-CN1
- ② = PB-CN2
- ③ = PB-CN3
- ④ = PB-CN4

| Test used for | A | B | Throat d/d |
|---------------|----------|--------|---------------|
| S-06-5 | 1.760 cm | 10° 0' | 4.08 |

Fig. 4 Semiscale tubular break simulator configuration.

The fluid properties, measured in the piping immediately upstream of the break location (PB-23, TFB-23, GB-23VR), were used as stagnation properties because of the low velocity (dynamic pressure) of the fluid at the measurement station. All the histories of stagnation thermodynamic states from which the data were taken contained a period of subcooled blowdown and saturated blowdown covering an appreciable range of quality. In addition to the measurements of fluid properties upstream of the break simulator, static pressures (PB-CN1) in the throat of two of the four nozzle break simulators and in the constant area section of the tubular break simulator were also measured. The mass flow rate was metered using a drag disk and turbine meter located in Spool 21 and a drag disk located just upstream of the break simulator insert in Spool 23^[a]. The range of the fluid conditions and inventory of the data that was available for each configuration is presented in Table I.

The pressure, temperature, and density measurement accuracies of the Semiscale data were ± 200 kPa, 2 K, and 8 kg/m^3 , respectively. Turbine meter and drag disk mass flow rate measurement accuracies are dependent upon the mass flow rate being measured. An estimate of the accuracy of Semiscale mass flow measurements, which is thought to be conservative, is ± 1 kg/s. This mass flow accuracy applies to most of the Semiscale data used in the study except for that from Test S-02-6 for which the instrumentation was overranged. Turbine meter mass flow rates exhibit errors larger than the quoted accuracy when the quality of the flow becomes greater than approximately 20%.

[a] Data from a test conducted with the drag disk in Spool 23 removed demonstrated that the presence of the device did not affect the flow rate.

TABLE I

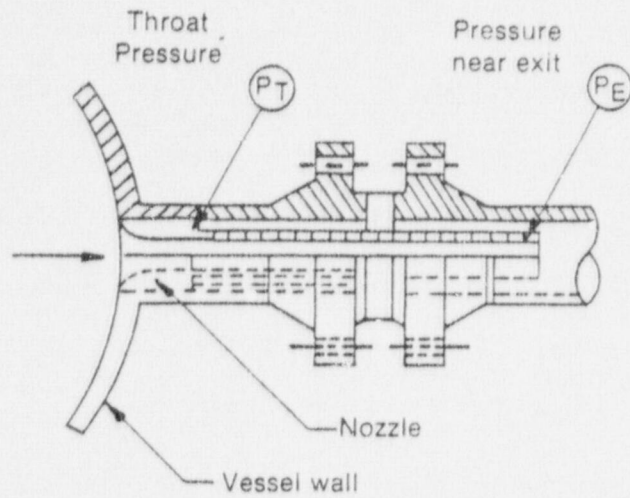
INVENTORY OF DATA POINTS AND STAGNATION FLUID PROPERTY RANGES
OBTAINED FROM SEMISCALE TESTS

| Test No. | Flow Passage | Throat Diameter (d_{th}) | Pressure Range (P_0) | Temperature Range (T_0) | Quality Range (x_0) | Void Fraction Range (α_0) | Maximum Subcooling | No. of Subcooled Data Points ($x_0 < 0$) | No. of Saturated Data Points ($x_0 \geq 0$) | No. of Data Points with ($0 < x_0 < 2\%$) | Data Time Interval |
|----------|-----------------------------|---------------------------------|-----------------------------|--------------------------------|----------------------------|---------------------------------------|--------------------|---|--|--|---------------------|
| | | cm | kPa | K | | | K | | | | s |
| S-05-6 | Converging-Diverging Nozzle | 2.451 | 10087 to 5804 | 573 to 547 | -0.0070 to +0.2746 | 0.0 to 0.9233 | 26 | 4 | 16 | 1 | 0.17 to 7.13 |
| S-02-4 | Converging-Diverging Nozzle | 1.760 | 10999 to 3268 | 571 to 512 | -0.0119 to +0.4922 | 0.0 to 0.9797 | 39 | 57 | 296 | 78 | 0.05 to 18.47 |
| S-29-1 | Converging-Diverging Nozzle | 1.311 | 10133 to 4885 | 566 to 536 | -0.0084 to +0.2989 | 0.0 to 0.9308 | 33 | 54 | 124 | 19 | 1.46 to 19.93 |
| S-02-6 | Converging-Diverging Nozzle | 0.429 | 13186 to 7150 | 564 to 560 | -0.0241 to +0.3006 | 0.0 to 0.8942 | 53 | 91 | 24 | 0 | 0.35 to 99.65 |
| S-06-5 | Constant Area Duct | 1.760 | 10253 to 2774 | 569 to 503 | -0.0086 to +0.2871 | 0.0 to 0.9600 | 32 | 91 | 49 | 8 | 0.17 to 20.00 |

2. GENERAL ELECTRIC EXPERIMENTS

The General Electric data that were used in the study were taken from Reference 11. The experiments reported in Reference 11 were performed by exhausting subcooled water or low-quality steam-water mixtures from a pressure vessel through various flow passages in which choking occurred. A schematic drawing depicting the test system is presented in Figure 5. The flow passages included a single-point throated, converging-diverging nozzle; tubes having length-to-diameter ratios of 0, 9, 18, and 50; and an orifice, all having a minimum diameter of 1.27 centimeters. The key dimensions of the configurations that were tested to generate the data used in the present study are shown in Figure 6.

Pressure and temperature in the vessel at the elevation of the penetration leading to the test duct hardware were measured. These measurements were used as the stagnation values. The density at the same location was derived by making a local differential pressure measurement. The static pressure was measured in the throat of the orifice and the nozzle. In the case of the tubes, the static pressure near the exit was measured. The mass flow rate was determined from the time rate of change of the fluid mass inventory in the vessel. The fluid mass inventory was determined from the liquid level based on differential pressure measurements in combination with the density of the fluid. The range of fluid conditions and an inventory of the data that were available for each test configuration is presented in Table II. The accuracy of the measurements was not stated in Reference 11.



Typical nozzle installed in pipe

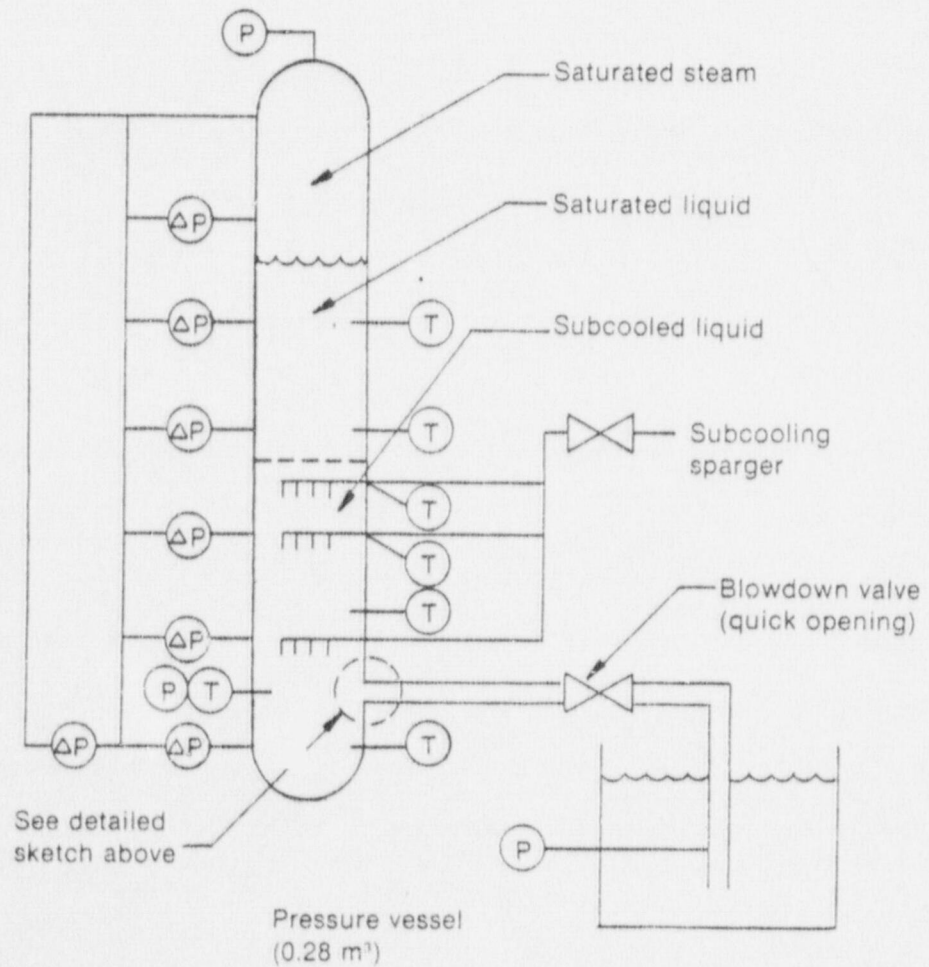


Fig. 5 Schematic of General Electric critical flow test equipment.

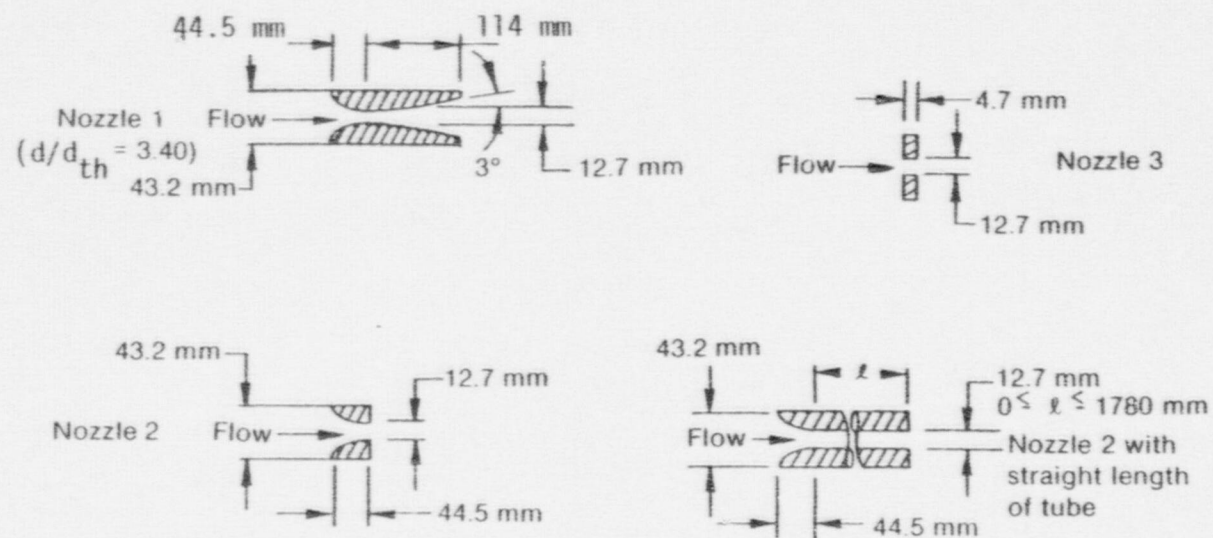


Fig. 6 General Electric critical flow test duct configurations.

TABLE II

INVENTORY OF DATA POINTS AND STAGNATION FLUID PROPERTY RANGES
OBTAINED FROM GENERAL ELECTRIC TESTS

| Flow Passage | Throat Diameter (d_{th}) | Pressure Range (p_o) | Temperature Range (T_o) | Quality Range (x_o) | Void Fraction Range (α_o) | Maximum Subcooling | No. of Subcooled Data Points ($x_o < 0$) | No. of Saturated Data Points ($x_o \geq 0$) |
|-------------------------------------|---------------------------------|-----------------------------|--------------------------------|----------------------------|---------------------------------------|--------------------|---|--|
| | cm | kPa | K | | | K | | |
| Converging-Diverging Nozzle | 1.270 | 7074 to 3034 | 559 to 492 | -0.0041 to +0.0080 | 0.0 to 0.1848 | 42 | 26 | 103 |
| Constant Area Duct $\ell/d = 0$ | 1.270 | 6757 to 5723 | 557 to 538 | -0.0021 to +0.0065 | 0.0 to 0.1338 | 18 | 3 | 10 |
| Constant Area Duct $\ell/d = 9$ | 1.270 | 6839 to 5764 | 557 to 542 | -0.0018 to +0.0033 | 0.0 to 0.0732 | 15 | 5 | 10 |
| Constant Area Duct $\ell/d = 18$ | 1.270 | 6984 to 5992 | 559 to 549 | -0.0008 to +0.048 | 0.0 to 0.0964 | 3 | 5 | 17 |
| Constant Area Duct $\ell/d = 5$ | 1.270 | 7129 to 5909 | 560 to 511 | -0.0044 to +0.0040 | 0.0 to 0.0769 | 44 | 49 | 47 |
| Orifice | 1.270 | 6805 to 4275 | 558 to 485 | -0.0059 to +0.0060 | 0.0 to 0.1325 | 69 | 18 | 40 |

IV. DISCUSSION OF RESULTS

The results of calculations made to determine critical flow multipliers for nozzle, tube, and orifice flow passages are discussed in this section. Critical flow multipliers and RMS percent deviations from the critical flow multipliers were derived from ratios of measured-to-calculated critical flow rates. The calculation of critical flow parameters including the mass flow ratios is not discussed in this section but is discussed in Appendix A. The discussion presented in this section is divided into three parts. In the first part, the suitability of each of the critical flow models for calculating critical flow rates occurring in particular flow passages when the stagnation conditions are in specified ranges are discussed. Computational accuracies exhibited by the model and a computational technique for use with tubular flow passages are also discussed. The discussion of the data presented in the first part treats each flow passage configuration independently of the other configurations. This same approach is maintained in the second part of the discussion, which covers the variation of the critical flow multiplier and accuracy values with the range of stagnation qualities corresponding to the data used in their determination. The last part of the discussion deals with the effect of flow passage geometry changes on the critical flow multipliers required for calculating critical flow rates occurring in a particular type of flow passage and on computational accuracy for the same type of flow passage configuration, i.e., nozzles and tubes.

1. BASIC CRITICAL FLOW CALCULATION CONSIDERATIONS

The critical flow data associated with each of the flow passage configurations were divided into three sets on the basis of stagnation universal quality. The three regimes of stagnation universal quality were: (a) negative universal qualities corresponding to subcooled conditions, (b) positive universal qualities between 0 and 2%, and (c) positive universal qualities greater than 2%. The ratios of measured mass flow rate to the critical mass flow rate calculated using a given critical flow model for a particular flow passage with stagnation conditions in one of the three regimes were averaged to produce a critical flow multiplier. The root-mean-square (RMS) deviations of the mass flow ratios from the critical flow multiplier were calculated and are presented as percentages of the corresponding critical flow multipliers. These percentages are equal to the root-mean-square of the percentage difference between measured and calculated mass flow rates [i.e. $(w_m - w_c')/w_c'$] and are referred to as "RMS percent deviations". In this form the RMS percent deviations are indices of calculational accuracy.

Critical flow multiplier and RMS percent deviation information are presented in Tables III, IV, and V. The data for each flow passage are divided into three categories in the tables on the basis of stagnation universal quality. The model which was found, by virtue of having the lowest RMS percent deviation, to be the most suitable for computing critical flows for each flow passage with stagnation conditions in one of the three categories is indicated in Tables III, IV, and V.

CRITICAL FLOW MULTIPLIER AND RMS PERCENT DEVIATION
DATA FOR NOZZLES

| | Critical Flow Multipliers ^(a) | | | RMS Percent Deviations | | |
|--|--|---------------------|---------------|----------------------------------|---------------------|-----------|
| | Subcooled | Transition | Saturated | Subcooled | Transition | Saturated |
| Semiscale Test S-05-6 $d/d_{th} = 1.76$, $d_{th} = 2.451$ cm | | | | | | |
| x_0 (%) | -0.70 to -0.20 | 1.47 ^(e) | 2.56 to 27.46 | | | |
| No. of points | 4 | 1 | 15 | | | |
| Critical Flow Model | | | | | | |
| HEM | 1.124 | 0.995 | 1.012 | 10.7% | --- | 3.2% |
| Henry-Fauske | 0.919 | 0.618 | 0.758 | 4.2% | --- | 8.9% |
| Modified Burnell | 0.942 | 0.891 | 0.982 | 3.8% | --- | 6.4% |
| Bernoulli/HEM ^(b) | 0.894 | 1.123 | 1.205 | 5.9% | --- | 3.2% |
| Bernoulli with p_a^* | 0.829 | 0.661 | 0.671 | 3.0% ^(d) | --- | 4.7% |
| Semiscale Test S-02-4 $d/d_{th} = 2.45$, $d_{th} = 1.760$ cm | | | | | | |
| x_0 (%) | -1.19 to -0.07 | 0.06 to 1.98 | 2.53 to 49.22 | | | |
| No. of points | 57 | 78 | 218 | | | |
| Critical Flow Model | | | | | | |
| HEM | 1.135 | 1.033 | 0.943 | 15.1% | 14.9% | 3.5% |
| Henry-Fauske | 0.973 | 0.614 | 0.692 | 5.8% | 13.2% | 7.5% |
| Modified Burnell | 0.977 | 0.822 | 0.806 | 8.1% | 16.5% | 4.5% |
| Bernoulli/HEM ^(b) | 0.987 | 1.007 | 1.004 | 5.4% | 7.9% | 3.5% |
| Bernoulli with p_a^* | 0.820 | 0.724 | 0.595 | 3.2% ^(d) with p_a^* | | |
| Semiscale Test S-29-1 $d/d_{th} = 3.29$, $d_{th} = 1.311$ cm | | | | | | |
| x_0 (%) | -0.8 to -0.06 | 0.10 to 1.98 | 2.27 to 29.89 | | | |
| No. of points | 54 | 19 | 105 | | | |
| Critical Flow Model | | | | | | |
| HEM | 1.321 | 1.349 | 0.964 | 25.8% | 23.1% | 22.5% |
| Henry-Fauske | 1.022 | 0.770 | 0.746 | 9.6% | 20.5% | 27.5% |
| Modified Burnell | 1.041 | 0.960 | 0.876 | 14.0% | 21.8% | 25.2% |
| Bernoulli/HEM ^(b) | 1.041 | 1.319 | 1.144 | 8.1% | 13.4% | 21.9% |
| Bernoulli with p_a^* | [c] | [c] | [c] | [c] | [c] | [c] |
| General Electric Nozzle 1 $d/d_{th} = 1.05$, $d_{th} = 1.270$ cm | | | | | | |
| x_0 (%) | -0.41 to -0.01 | 0.10 to 0.80 | --- | | | |
| No. of points | 26 | 103 | 0 | | | |
| Critical Flow Model | | | | | | |
| HEM | 1.520 | 1.674 | No data | 24.7% | 20.6% | No data |
| Henry-Fauske | 1.139 | 0.890 | No data | 6.5% | 16.2% | No data |
| Modified Burnell | 1.128 | 1.055 | No data | 11.6% | 14.1% | No data |
| Bernoulli/HEM ^(b) | 0.997 | 0.942 | No data | 6.1% | 12.8% | No data |
| Bernoulli with p_a^* | 0.920 | 0.852 | No data | 6.1% ^(d) | 6.8% ^(d) | No data |
| Semiscale Test S-02-6 $d/d_{th} = 10.07$, $d_{th} = 0.429$ cm | | | | | | |
| x_0 (%) | -2.41 to -0.08 | -- | 3.63 to 30.06 | | | |
| No. of points | 91 | 0 | 24 | | | |
| Critical Flow Model | | | | | | |
| HEM | 1.862 | No data | 1.776 | 29.2% | No data | 8.8% |
| Henry-Fauske | 1.425 | No data | 1.357 | 13.0% | No data | 4.7% |
| Modified Burnell | 1.432 | No data | 1.798 | 17.9% | No data | 5.1% |
| Bernoulli/HEM ^(b) | 1.75 | No data | 2.114 | 7.0% | No data | 8.8% |
| Bernoulli with p_a^* | [c] | No data | [c] | [c] | No data | [c] |

(a) For a given quality regime, the model indicated with boxes around the multiplier provided the best representation of the data, based on minimum RMS percent deviation. For all three quality regimes considered together, the model indicated by double lines under the multipliers provided the best representation of the data.

(b) Bernoulli/HEM calculations were made with critical flow multipliers of 0.83 and 0.84 respectively applied to the mass flow rates calculated using the individual Bernoulli and HEM models. The absolute multipliers to be applied to the Bernoulli and HEM models for subcooled and saturated stagnation conditions are the product of the table values and the multipliers that were used to make the calculations.

(c) Measured throat pressures were not available; therefore, the calculation with the Bernoulli mass flux expression could not be made.

(d) The Bernoulli mass flux expression with the measured throat pressure input for critical pressure, although not a critical flow model, has produced mass flow (flux) ratios having the smallest RMS percent deviation from the corresponding critical flow multiplier.

(e) Only one data point was available with stagnation quality in this regime.

TABLE IV
CRITICAL FLOW MULTIPLIER AND RMS PERCENT DEVIATION
DATA FOR TUBES

| | Critical Flow Multipliers ^(a) | | | RMS Percent Deviations | | |
|--|--|--------------|---------------|------------------------|---------------------|---------------------|
| | Subcooled | Transition | Saturated | Subcooled | Transition | Saturated |
| General Electric Nozzle 2, $L/d = 0$ $d = 1.270$ cm, $L = 0$ cm | | | | | | |
| x_0 (%) | -0.21 to -0.06 | 0.0 to 0.65 | --- | | | |
| No. of points | 3 | 10 | 0 | | | |
| Critical Flow Model | | | | | | |
| HEM | 1.890 | 1.908 | No data | 18.0% | 11.3% | No data |
| Henry-Fauske | 1.332 | 1.056 | No data | 3.6% | 9.3% | No data |
| Modified Burnell | 1.357 | 1.318 | No data | 4.9% | 9.7% | No data |
| Bernoulli/HEM ^(b) | <u>1.114</u> | <u>1.326</u> | No data | 3.5% | 9.0% | No data |
| Bernoulli with P^*_m | 1.126 | 0.907 | No data | 4.9% | 5.0% ^(d) | No data |
| Semiscale Test S-06-5, $L/d = 4$ $d = 1.260$ cm, $L = 7.186$ cm | | | | | | |
| x_0 (%) | -0.06 to -0.23 | 0.46 to 1.25 | 2.13 to 28.71 | | | |
| No. of points | 9 | 8 | 41 | | | |
| Critical Flow Model | | | | | | |
| HEM | 0.995 | 1.054 | <u>1.115</u> | 4.6% | 2.8% | 3.8% |
| Henry-Fauske | 0.872 | <u>0.634</u> | 0.897 | 3.7% | 1.6% | 14.4% |
| Modified Burnell | <u>0.865</u> | 0.861 | 1.031 | 2.6% | 4.0% | 9.5% |
| Bernoulli/HEM ^(b) | 0.728 | 0.944 | <u>1.115</u> | 6.6% | 3.9% | 3.8% |
| Bernoulli with P^*_m | 0.930 | 0.849 | 0.798 | 2.3% ^(d) | 5.5% | 3.6% ^(d) |
| General Electric Nozzle 2, $L/d = 9$ $d = 1.270$ cm, $L = 11.430$ cm | | | | | | |
| x_0 (%) | -0.18 to -0.03 | 0.08 to 0.33 | --- | | | |
| No. of points | 5 | 10 | 0 | | | |
| Critical Flow Model | | | | | | |
| HEM | 1.144 | 1.161 | No data | 14.6% | 7.8% | No data |
| Henry-Fauske | <u>0.814</u> | 0.635 | No data | 2.4% | 6.1% | No data |
| Modified Burnell | 0.836 | <u>0.798</u> | No data | 5.9% | 4.7% | No data |
| Bernoulli/HEM ^(b) | 0.675 | 0.724 | No data | 3.1% | 8.9% | No data |
| Bernoulli with P^*_m | [c] | [c] | No data | [c] | [c] | No data |
| General Electric Nozzle 2, $L/d = 18$ $d = 1.270$ cm, $L = 22.860$ cm | | | | | | |
| x_0 (%) | -0.03 to -0.04 | 0.10 to 0.48 | --- | | | |
| No. of points | 5 | 17 | 0 | | | |
| Critical Flow Model | | | | | | |
| HEM | 1.220 | 1.019 | No data | 3.5% | 4.4% | No data |
| Henry-Fauske | <u>0.704</u> | <u>0.567</u> | No data | 1.8% | 3.1% | No data |
| Modified Burnell | 0.570 | 0.723 | No data | 4.8% | 3.4% | No data |
| Bernoulli/HEM ^(b) | 0.566 | 0.713 | No data | 2.0% | 11.4% | No data |
| Bernoulli with P^*_m | 0.589 | 0.466 | No data | 3.2% | 6.1% | No data |
| General Electric Nozzle 2, $L/d = 50$ $d = 1.270$ cm, $L = 63.500$ cm | | | | | | |
| x_0 (%) | -0.44 to -0.01 | 0.05 to 0.40 | --- | | | |
| No. of points | 49 | 47 | 0 | | | |
| Critical Flow Model | | | | | | |
| HEM | 0.749 | 0.881 | No data | 10.7% | 4.6% | No data |
| Henry-Fauske | 0.570 | 0.490 | No data | 11.4% | 4.4% | No data |
| Modified Burnell | <u>0.570</u> | <u>0.612</u> | No data | 6.3% | 4.3% | No data |
| Bernoulli/HEM ^(b) | 0.495 | 0.586 | No data | 16.9% | 13.9% | No data |
| Bernoulli with P^*_m | 0.597 | No data | No data | 9.0% | No data | No data |

(a) For a given quality regime, the models indicated with boxes around the multiplier provided the best representation of the data, based on minimum RMS percent deviations. For all three quality regimes considered together, models indicated by double lines under the multipliers provided the best representation of the data.

(b) Bernoulli/HEM calculations were made with critical flow multipliers of 0.83 and 0.84 respectively applied to the mass flow rates calculated using the individual Bernoulli and HEM models. The absolute multipliers to be applied to the Bernoulli and HEM models for subcooled, saturated stagnation conditions are the product of the table values and the multipliers that were used to make the calculations.

(c) Measured throat pressures were not available; therefore, the calculation with the Bernoulli mass flux expression could not be made.

(d) The Bernoulli mass flux expression with the measured throat pressure input for critical pressure, although not a critical flow model, has produced mass flow (flux) ratios having the smallest RMS percent deviation from the corresponding critical flow multiplier.

TABLE V

CRITICAL FLOW MULTIPLIER AND RMS PERCENT DEVIATION
DATA FOR AN ORIFICE

| General Electric Nozzle 3 d = 1.270 cm, $\beta = 0.294$ | | | | | | |
|--|--|-------------|-----------|------------------------|---------------------|-----------|
| x_o (%) | Critical Flow Multipliers ^[a] | | | RMS Percent Deviations | | |
| | Subcooled | Transition | Saturated | Subcooled | Transition | Saturated |
| x_o (%) | -0.59 to -0.02 | 0.0 to 0.60 | --- | | | |
| No. of points | 18 | 40 | 0 | | | |
| Critical Flow Model | | | | | | |
| HEM | 1.214 | 1.721 | no data | 32.1% | 8.7% | no data |
| Henry-Fauske | 0.935 | 0.941 | no data | 11.7% | 5.5% | no data |
| Modified Burnell | 0.933 | 1.143 | no data | 18.9% | 6.0% | no data |
| Bernoulli/HEM ^[b] | 0.828 | 1.213 | no data | 4.3% | 10.5% | no data |
| Bernoulli with p_m^* | 0.672 | 0.652 | no data | 2.0% ^[c] | 2.4% ^[c] | no data |

[a] For a given quality regime, the model indicated with a box around the multiplier provided the best representation of the data, based on minimum RMS percent deviation. For all quality regimes considered together, the model indicated by double lines under the multipliers provided the best representation of the data.

[b] Bernoulli/HEM calculations were made with critical flow multipliers of 0.83 to 0.84 respectively applied to the mass flow rates calculated using the individual Bernoulli and HEM models. The absolute multipliers to be applied to the Bernoulli and HEM models for subcooled and saturated stagnation conditions are the product of the table values and the multipliers that were used to make the calculations.

[c] The Bernoulli mass flux expression with the measured throat pressure input for critical pressure, although not a critical flow model, has produced mass flux ratios having the smallest RMS percent deviation from the corresponding critical flow multiplier.

The critical flow multiplier corresponding to the most suitable model for each range of stagnation conditions is enclosed in a box. The critical flow model which is considered the most suitable for predicting critical flow rates occurring in a particular flow passage for all stagnation conditions is indicated by underlining of the values corresponding to that model. The number of data points that were available in each of the three stagnation quality regimes and the actual range of stagnation universal qualities spanned by the data in each stagnation quality regime are indicated in Tables III, IV, and V for each flow passage.

In both Tables III and IV, the data presented for a given quality regime were not evaluated using data spanning exactly the same range. The data presented in the next section will show that RMS percent deviation and critical flow multiplier can vary significantly, depending on the range of the stagnation quality data. For this reason, the data presented for the various configurations in Tables III and IV cannot be legitimately compared in most cases. The values in Tables III, IV, and V are those derived using the largest range of stagnation conditions for which data were available.

Despite the differences in the actual stagnation quality ranges, trends in the suitability of the models for predicting critical flow rates in nozzles and tubes are identifiable in the data presented in Tables III and IV. The Bernoulli/HEM model is indicated to be the most suitable for predicting critical flow rates in all five of the nozzle

configurations, because of the consistently low values of the Bernoulli/HEM RMS percent deviations. However, even better predictions than those obtained using the Bernoulli/HEM model could be obtained using the Bernoulli mass flux expression for subcooled and transition conditions, if the critical pressure could be accurately predicted. The conditions for which the Bernoulli mass flux expression produced superior accuracies are indicated by a footnote.

No one critical flow model was found to be consistently the most suitable for predicting critical flow rates occurring in tubular flow passages. However, close examination of the data for tubular configurations shows that, while the Henry-Fauske model did not produce the lowest RMS percent deviation values for all configurations, it did produce values quite close to the lowest values in nearly every case. If a single model had to be selected to produce predictions in the best agreement with critical flow rates occurring in constant area ducts for subcooled and very low quality ($x_o \leq 2\%$) stagnation conditions, the Henry-Fauske model is indicated to be the best choice. The same good performance might well not be exhibited if more data were available for saturated stagnation conditions having qualities greater than 2%, because the equilibrium conditions might well exist at the choke point in contrast to the Henry-Fauske assumption of nonequilibrium at the choke point. An indication that this would be the case is shown by the fact that, for Semiscale Test S-06-5, the Henry-Fauske RMS percent deviation for saturated conditions is the highest value listed. Interestingly, the HEM index for the same conditions is the lowest.

The prospective user of the information listed in Table IV must consider the fact that the critical flow calculations upon which the critical flow multiplier values are based were made without accounting for viscous pressure losses in the tubes. These losses could have been accounted for, but would have required iterative calculations which were beyond the scope of the study. Check calculations showed that accounting for pressure losses in making the calculations could significantly change the values of the calculated flow rates or fluxes and subsequently change the derived critical flow multiplier value when the stagnation conditions were subcooled. Since the viscous losses were not accounted for in determining the critical flow multipliers, the effect of the viscous losses has been incorporated in the tubular critical flow multiplier values listed in Table IV. For this reason, the piping between an effective plenum such as the vessel and the break location should not be nodalized in a system calculation if the values listed in Table IV are used, because the pressure losses would effectively be accounted for twice - once in the critical flow multiplier and once in the system calculations. The proper use of the tubular critical flow multipliers in Table IV would be to select a multiplier value on the basis of the length-to-diameter ratio of the pipe connecting the closest effective plenum and the break location. The choking location would then be considered to be at the exit closest to the break from the volume which was used to model that part of the system which forms an effective plenum.

The most suitable model for use in predicting critical flows in orifices could not be conclusively determined, since data generated with

only one orifice was used in the study. The data for the orifice presented in Table V are nonetheless noteworthy. Calculations made with the Bernoulli mass flux expression, in which measured orifice pressures were used as critical pressures, produced the lowest RMS percent deviations listed. These results indicate that at least for subcooled and very low quality stagnation conditions the Bernoulli mass flux expression could be used to predict critical flow rates through orifices with a good degree of accuracy if an accurate analytical expression were available for predicting the critical pressure. It is also interesting to note that the critical flow multiplier values calculated for the Bernoulli mass flux expression are in the sixty percentiles, which is typical of single-phase orifice coefficients.

The Bernoulli/HEM model produced critical mass fluxes in the best agreement with the measured values, while the homogeneous equilibrium model produced values in the worst agreement with the measured values when the stagnation conditions were subcooled. The net multiplier for the Bernoulli/HEM model for subcooled conditions was 0.69 (i.e. $0.83 * 0.828$) which is a typical orifice coefficient value. These results indicate that a nonequilibrium state existed at the choke point. The basic data presented in Appendix A shows that the empirically derived expression for critical pressure ratio used in connection with the Bernoulli/HEM model produced critical pressures that were in the best agreement with the measured pressures and exhibited the same trend as the measured values.

The Bernoulli/HEM model did not, however, produce critical mass fluxes in the best agreement with measured values for very low quality

stagnation conditions. This result is probably due in part to conditions at the choke point remaining in nonequilibrium, while the calculated values were quality weighted averages of mass fluxes produced by one model which assumes nonequilibrium at the choke point and another model which assumes the existence of equilibrium conditions at the choke point. Calculations made using only the Bernoulli mass flow rate would have produced critical mass fluxes in better agreement with the measured values.

The Henry-Fauske model actually produced the mass fluxes that were in the best agreement with the measured values for very low stagnation qualities. The result must be regarded with some degree of caution because Table V shows that the Henry-Fauske critical flow multiplier for the transition quality regime was 0.941 instead of a value in the sixty percentiles. The basic data presented in Appendix A also shows that the agreement between the Henry-Fauske critical pressures and the measured orifice pressure is quite poor. The good agreement between the Henry-Fauske critical mass fluxes and the measured values is suspected to be fortuitous. It is possible that the high critical pressure predictions which would have produced mass fluxes that were low were compensated for by use of the actual orifice area in making the calculations rather than accounting for the flow area reduction at the choke point caused by the formation of a vena contracta.

The good performance of the Bernoulli/HEM model for subcooled conditions and the questionable nature of the performance of the Henry-Fauske model for stagnation conditions having very low qualities leads

to a recommendation to use the Bernoulli/HEM model for the prediction of critical flow rates through orifices in situations when it is known that the stagnation conditions will be both subcooled and saturated with very low quality. Use of a large transition quality like 10% will help ensure that mass flow rates calculated at very low qualities are primarily the result of nonequilibrium calculations.

Identification of the critical flow model which can best be used to predict critical flow rates in each of the three types of flow passages for which data was used in the study leads to an interesting question. Which of the models can best be considered a multipurpose critical flow model with the proviso that the selected model must currently be available in the RELAP4 code? The RMS percent deviations for nozzle flow passages presented in Table III show that a Henry-Fauske/HEM combination critical flow model would produce results nearly as good as those produced by the Bernoulli/HEM model, which is not presently available as a RELAP4 critical flow model option. Critical flows occurring in tubular flow passages were found to be best predicted over the full range of fluid conditions (subcooled through high quality saturated) using a combination of the Henry-Fauske model for subcooled stagnation conditions and the homogeneous equilibrium model for saturated stagnation conditions, according to the information presented in Table IV. For orifice flow passages, Table V shows that fair to good predictions can be produced using a Henry-Fauske/HEM model for subcooled and transition conditions, but due to the lack of data, no assessment was made of the accuracy with which HEM can predict critical flow rates through orifices at saturated stagnation conditions. If a multipurpose critical flow model which is currently available in RELAP4 were to

be selected, the information presented in Tables III, IV, and V indicate that the Henry-Fauske/HEM combination critical flow model would be the best choice. However, this selection must be made with some reservation because only calculational accuracies of individual models were assessed in the study, with the exception of the Bernoulli/HEM model. The Henry-Fauske/HEM critical flow model option currently available in RELAP4 calculates critical flow rates using a quality-weighted average similar to that expressed by Equation (1) when the stagnation quality is between zero and the user-selected transition quality. The calculational accuracies of the Henry-Fauske/HEM and Modified Burnell/HEM combination models for transition stagnation conditions were not investigated in the study, although performance in the transition regime may be important in particular cases. Selection of the Henry-Fauske/HEM model instead of the Modified Burnell/HEM model may be inappropriate in cases where the stagnation quality at the break remains in the transition regime for an extended period of time. Nonetheless, based on the currently available data, the Henry-Fauske/HEM model is the best choice for a multipurpose critical flow model currently available in the RELAP4 code. It should still be remembered that calculational accuracies better than those exhibited by the Henry-Fauske and HEM models can be attained in some cases by using a critical flow model and associated multiplier values that have been shown to be the most suitable for a particular flow situation.

The data presented in Tables III, IV, and V, along with that presented in the other two subsections of this section, are intended to be used in the selection and application of critical flow models for performing system model calculations. However, the user should keep certain infor-

mation in mind when applying these data. Interpretation of the RMS percent deviation data is dependent on the type of probability density distribution.

The probability distributions of the mass flow ratios that were generated during the study are not presented in this report due to the lack of sufficient data to properly define the probability distributions in general; however, the probability distributions that were generated using the larger sets of data were approximately normal distributions and the RMS deviation therefore approximates one standard deviation. It should be remembered that even if all the distributions were normal, values beyond the quoted calculational accuracies will occur 32% of the time if a large number of calculations are made. On the other hand, the RMS deviations quoted are probably conservatively high since they reflect random measurement errors as well as model inaccuracy.

It is important to note that there is a difference between the critical flow prediction accuracies of "component" critical flow models of the type which were obtained in this study and the critical flow prediction accuracies that can be obtained when these component models are used in an integral system model. In the study performed, the input stagnation conditions were known to correspond to the critical flow rates which were being predicted. In a system model calculation, the predicted critical flow rates depend upon the predicted stagnation property values which are used as input to the critical flow model. If the input stagnation property values are wrong due to mismodeling in other system model components, the critical flow rate predictions can be in error even if a perfectly accurate

critical flow model were used to predict the flow rates. The calculational accuracy estimates generated in this study did not account for possible input stagnation property errors.

2. THE EFFECT OF STAGNATION QUALITY RANGE

Two key questions exist about the use of the data presented in Tables III, IV, and V. Answering these questions requires having information about the dependency of critical flow multiplier and RMS percent deviation values on the range of stagnation qualities covered by data used in their derivation. One question is whether the values listed in Tables III, IV, and V, which were derived using data spanning the largest range of stagnation qualities for which data was available, can be used if it is known that stagnation qualities in a proposed system calculation will span different ranges of qualities. Another question is whether the critical flow multiplier and RMS percent deviation values exhibit some simple dependence upon a geometric characteristic of flow passages of a particular type. This dependence could only be explored by comparing critical flow multipliers and RMS percent deviation values derived using data covering the same range. The question of geometry dependence is discussed in the next subsection.

Information about stagnation quality range dependence was obtained by computing critical flow multiplier and RMS percent deviation values using subsets of the available data contained in successively larger stagnation quality ranges having zero quality as one boundary. The values thus derived were plotted against the upper (lower in the case of negative universal qualities) limit of the quality range. The plots of this type generated

using Bernoulli/HEM data and Henry-Fauske data for nozzle and tubular flow passages, respectively, are presented and discussed in Appendix B. These models were selected because they most consistently produced critical flow rates in relatively good agreement with the measured values. The question of the utility of the data presented in Tables III and IV for different ranges of stagnation quality is discussed in this subsection.

The variations in the values of critical flow multipliers and corresponding RMS percent deviations with changes in stagnation quality range within specified limits are listed in Table VI. These data summarize the data presented in Appendix B in which critical flow multiplier and RMS percent deviation values are plotted versus stagnation quality range boundary. The stagnation quality ranges were divided into two or three groups depending upon the overall quality range spanned by the available data or the appropriateness of performing critical flow calculations with two or three stagnation quality regimes. The data for Semiscale Test S-05-6 will be used as an example. Since sufficient data was available and indicated critical flow rates could be most accurately calculated by defining three stagnation quality regimes as discussed in Appendix B, three sets of data are presented in Table VI for Test S-05-6. The first set of quality regime limits are -0.010 to 0.0 . Data spanning different quality ranges within these limits were used to calculate values of the critical flow multiplier and the corresponding RMS percent deviation. These calculations resulted in minimum and maximum values for the critical flow multiplier and the RMS percent deviation. It is important to note that minimum and maximum values of the critical flow multiplier and RMS percent deviation do not necessarily correspond to one another, but are simply the minimum and maximum values that were obtained using data in quality ranges contained

TABLE VI

VARIATION IN CRITICAL FLOW MULTIPLIERS AND RMS PERCENT DEVIATIONS

| Converging-Diverging Nozzle Flow Passages | | | Tubular Flow Passages | | |
|--|--|---------------------------------------|---|--|---------------------------------------|
| Bernoulli/HEM Critical Flow Model ^(a) | | | Henry-Fauske Critical Flow Model ^(b) | | |
| Quality Range Limit Variation | Critical Flow Multiplier Variation | RMS Percent Deviation Variation | Quality Range Limit Variation | Critical Flow Multiplier Variation | RMS Percent Deviation Variation |
| Semiscale Test S-05-6 $d'/d_{th} = 1.76$ | | | General Electric Nozzle 2 $L/d = 0$ | | |
| -0.010 to 0.0 | 0.867 to 0.894 | 5.9 to 7.3% | -0.003 to 0.0 | 1.324 to 1.359 | 2.6 to 3.7% |
| 0.0 to 0.060 | 1.123 to 1.190 | 2.9 to 4.8% | 0.0 to 0.007 | 1.056 to 1.322 ^(e) | 9.3 to 9.7% |
| 0.060 to 0.300 | 1.200 to 1.230 ^(c) | 0.0 to 2.0% | | | |
| Semiscale Test S-02-4 $d/d_{th} = 2.45$ | | | Semiscale Test S-06-5 $L/d = 4$ | | |
| -0.010 to 0.0 | 0.967 to 0.978 | 5.5 to 7.0% | -0.010 to 0.0 | 0.847 to 0.872 | 2.6 to 3.7% |
| 0.0 to 0.020 | 1.031 to 1.081 | 8.0 to 14.1% | 0.0 to 0.020 | 0.632 to 0.661 | 1.8 to 2.2% |
| 0.020 to 0.492 | 1.004 ^(d) | 3.5% | 0.020 to 0.287 | 0.897 ^(d) | 14.4% |
| Semiscale Test S-29-1 $d/d_{th} = 3.29$ | | | General Electric Nozzle 2 $L/d = 9$ | | |
| -0.010 to 0.0 | 1.041 to 1.083 | 6.3 to 8.1% | -0.002 to 0.0 | 0.804 to 0.814 ^(c) | 2.4% ^(d) |
| 0.0 to 0.020 | 1.320 to 1.440 | 10.6 to 13.4% | 0.0 to 0.004 | 0.636 to 0.692 | 0.8 to 6.1% |
| 0.020 to 0.300 | 1.164 ^(d) [f] | 21.9% ^(d) [f] | | | |
| General Electric Nozzle 1 $d/d_{th} = 3.40$ | | | General Electric Nozzle 2 $L/d = 18$ | | |
| -0.004 to 0.0 | 0.984 to 0.997 | 6.1 to 7.9% | -0.001 to 0.0 | 0.700 ^(d) | 1.8% ^(d) |
| 0.0 to 0.008 | 0.912 to 1.022 | 4.3 to 12.8% | 0.0 to 0.005 | 0.567 to 0.607 | 0.6 to 3.1% |
| Semiscale Test S-02-6 $d/d_{th} = 10.07$ | | | General Electric Nozzle 2 $L/d = 50$ | | |
| -0.010 to 0.0 | 1.432 to 1.496 ^(g) | 6.0 to 7.0% ^(g) | -0.005 to 0.0 | 0.493 to 0.570 | 6.3 to 11.4% |
| 0.0 to 0.400 | 2.114 to 2.794 ^(g) | 8.4 to 10.5% ^(g) | 0.0 to 0.005 | 0.467 to 0.490 | 0.2 to 6.9% |

[a] The Bernoulli/HEM model was selected from the models considered in this study because it provided the best agreement to all of the converging-diverging nozzle data in the maximum quality ranges available, based on RMS percent deviation data.

[b] The Henry-Fauske model was selected from the models considered in this study because it provided the best agreement to all of the tube data in the maximum quality ranges available, based on RMS percent deviation data.

[c] Range was estimated from a plot of mass flow ratio as a function stagnation universal quality.

[d] Data on the variation of the critical flow multiplier and RMS percent deviation with quality range are not available. The values shown corresponds to the maximum quality range for which data were available.

[e] The maximum critical flow multiplier value was derived from a stagnation quality range containing only one data point and is therefore questionable. The next highest value of the multiplier was based on more data and is 1.142.

[f] These values were derived using questionable data. Better values corresponding to a stagnation quality range of 0.020 to 0.100 are a critical flow multiplier of 1.000 and RMS percent deviation of 10.0.

[g] These data are suspect because of questions about the mass flow measurement accuracy.

in the specified limits. Comparison of the data presented in Tables III and VI for Test S-05-6 shows that the use of a critical flow multiplier of 0.894 from Table III would be a good choice for performing critical flow calculations over stagnation universal quality ranges from zero down to as low as -0.010; since the lowest value of the critical flow multiplier recorded was 0.867^[a]. The RMS percent deviations varied from a minimum of 5.9 to a maximum of 7.3%. Unfortunately, it can not be simply assumed that critical flow rates in the Test S-05-6 flow passage or similar flow passage geometry can be calculated to within at most $\pm 7.3\%$ error for subcooled conditions. The RMS percent deviations represent calculational accuracies that can be expected only if a particular critical flow multiplier is used. It is conceivable that use of the critical flow multiplier value of 0.894 could result in calculational errors of approximately $\pm 10\%$ instead. This would occur if calculations were to be made over a range of stagnation qualities equal to the range of qualities spanned by the data that produced the critical flow multiplier value of 0.867. Furthermore, if the RMS percent deviation corresponding to the 0.867 value was $\pm 7.3\%$, use of a 0.894 critical flow multiplier instead would produce values that were an additional 3% too high. The calculation accuracy band would be biased by 3% and would approximately span from +4 to -10%. In cases where the choice of the critical flow multiplier from Tables III and IV does not produce acceptable calculational accuracy estimates using the approach just discussed, more specific information about the values of the critical flow multiplier and corresponding RMS percent deviation can be obtained from the plots presented in Appendix B.

[a] A critical flow multiplier value specifically suited for a specific quality range can be obtained from plots presented in Appendix B.

Several significant facts are illustrated by the data presented in Table VI. The values of critical flow multipliers which exhibit variations greater than 0.1 and values of RMS percent deviations greater than 10% are enclosed in boxes in Table VI. There are notably few of these boxes and all of the values which exceed the aforementioned limits do so for reasons which are at least understood and could conceivably be corrected. The reasons for the large critical flow multiplier variations and RMS percent deviations will be discussed later in this section. Ignoring the boxed values, the data presented in Table VI shows that critical flow rates in the nozzle configurations could be calculated to within $\pm 6\%$, on the average, if a critical flow multiplier value commensurate with the range of stagnation qualities over which calculations are to be made is used. An expected average accuracy for tubular flow passages defined by the same method and subject to the same restrictions is $\pm 4.5\%$. If the worst choice of critical flow multiplier value is made^[a] and the maximum RMS percent deviation corresponds to the range of stagnation qualities over which calculations are to be made, the average error that would occur in computing critical flow rates for nozzle and tubular flow passages would be $\pm 8\%$, with the highest value being $\pm 14\%$. The boxed values were not used in calculating these average accuracies for reasons which will be discussed next.

The boxed data in Table VI exceeded the arbitrarily set limits of 0.1 variation in the critical flow multiplier or $\pm 10\%$ in the RMS percent deviation. In all of the cases where these limits were exceeded, some

[a] The worst choice in critical flow multiplier value would result from the selection of the maximum multiplier value listed in Table VI when the minimum value should have been selected or visa versa.

information was known which made the results understandable. This information concerned the data used to perform the calculations or the manner in which the calculations were made. With the exception of the Semiscale Test S-02-6 critical flow multipliers for saturated conditions, the critical flow multipliers that varied more than 0.1 were for very low quality, saturated stagnation conditions. These conditions have been identified in Reference 1 as conditions for which the nature of the flow process is changing from one in which nonequilibrium conditions exist at the choke point to one in which equilibrium is achieved at the choke point. It should be remembered that the Bernoulli/HEM model utilizes a weighted average technique when making the transition from computing critical flows using the Bernoulli model to computing critical flows using the homogeneous equilibrium model. This approach, while it limits the computed critical flow rates to values between reasonable upper and lower limits, does not produce values derived from fundamental physical principles. This is probably why sizable variations in the values of the critical flow multipliers and/or large values of RMS percent deviations were obtained for Semiscale Tests S-02-4 and S-29-1 and for the General Electric Nozzle 1 for stagnation conditions having qualities between 0 and 2%. The boxed data for Semiscale Tests S-02-6 and S-29-1 for saturated conditions are quite possibly the result of break flow measurement errors as discussed in Appendix A. The large variation in the value of the subcooled critical flow multiplier for General Electric Nozzle 2, $z/d = 0$, is the result of computing a critical flow multiplier using a range stagnation quality range that contained only one data point. Neglecting this value and using only data generated using several data points results in a range of multiplier values from 1.056 to

1.142. The large RMS percent deviation value listed for Semiscale Test S-06-5 for stagnation conditions having qualities greater than 2% is probably the result of the Henry-Fauske assumption of nonequilibrium at the choke point for conditions at which equilibrium has actually been achieved. The assumption of nonequilibrium at the choke point results in the use of stagnation densities to compute critical flow rates consequently producing values that are in poor agreement with observed values in situations where equilibrium has been reached at the choke point. The achievement of equilibrium at the choke point is accompanied by a significant amount of mass transfer, which results in densities lower than stagnation values and invalidates the assumption of a constant density flow process. Use of the homogeneous equilibrium model for the same conditions yields an acceptable RMS percent deviation value of $\pm 3.5\%$. The large RMS percent deviation value listed in Table VI as the maximum value obtained using General Electric Nozzle 2, $\ell/d = 50$, data at subcooled conditions is the result of not accounting for viscous losses in performing the critical flow calculations^[a].

3. THE EFFECT OF FLOW PASSAGE GEOMETRIC PARAMETERS

In this section the effect of geometric parameters on the values of critical flow multipliers associated with and calculational accuracy of each of the models is discussed. The discussion has been divided into two subsections: one dealing with nozzle flow passages and one dealing with tubular flow passages. Data showing the effect of nozzle diameter

[a] The question of accounting for viscous losses in performing critical flow calculations for tubular flow passages is discussed in Appendix B.

ratio upon critical flow multipliers and calculational accuracy is presented. For the tubular flow passages, the independent variable used in presenting the effect of flow passage geometry is length-to-diameter ratio. The use of nondimensional parameters as independent variables instead of actual dimensions cannot be satisfactorily justified at this time due to a lack of sufficient data. Use of length-to-diameter ratio as a characteristic parameter for tubular flow passages is discussed in Appendix A.

The approach taken in the presentation is to show the effect of the geometric parameter on the value of the critical flow multiplier needed to compute critical flow rates from stagnation conditions having qualities in one of the three specified regimes. These quality regimes are the same ones that have been discussed previously: subcooled, transition, and saturated. In order to allow comparison of critical flow multipliers and calculational accuracy values associated with different values of the geometric parameter, multiplier and accuracy index values determined using mass flow ratios spanning approximately the same range of stagnation conditions were used. For this reason the data presented in this subsection differs from that presented in Tables III and IV, although in general the differences are slight.

3.1 Nozzle Flow Passages

The effect of nozzle diameter ratio on the value of the critical flow multiplier and the associated calculational accuracy are presented in this subsection. The discussion is divided into three parts, each discussing the effect of nozzle diameter ratio on critical flow multiplier

value and corresponding calculational accuracy associated with calculating critical flow rates in a particular quality regime.

3.1.1 Subcooled Conditions. The variation in critical flow multiplier for use in computing critical flow rates in nozzles with subcooled stagnation conditions is presented in Figure 7 as a function of nozzle diameter ratio. All of the data presented were calculated using data having stagnation universal qualities approximately covering the range from zero to -0.5%. The data presented in Figure 7 shows good agreement between the critical flow multipliers determined using data measured in Semiscale and General Electric experiments with nozzles of similar geometry and nearly the same nozzle diameter ratio. The geometries of the Semiscale and General Electric nozzles are presented in Figures 3 and 6, respectively.

The critical flow multipliers associated with all of the models and the Bernoulli mass flux expression presented in Figure 7 are monotonically increasing. These results, which do not show any evidence of the critical flow multiplier value decreasing with increasing diameter ratio, may be misleading. The break flow rates measured in Semiscale Test S-02-6 may have been too high as discussed in Appendix A. The lower mass flow rates that were calculated using a mass balance would have resulted in the Test S-02-6 critical flow multipliers being lower. It is intuitively conceivable that the values of the critical flow multipliers might actually reach a maximum and decline for smaller throats, because as the size of the throat is reduced, separation zones (if they exist) and the boundary layer displacement thicknesses account for larger fractions of

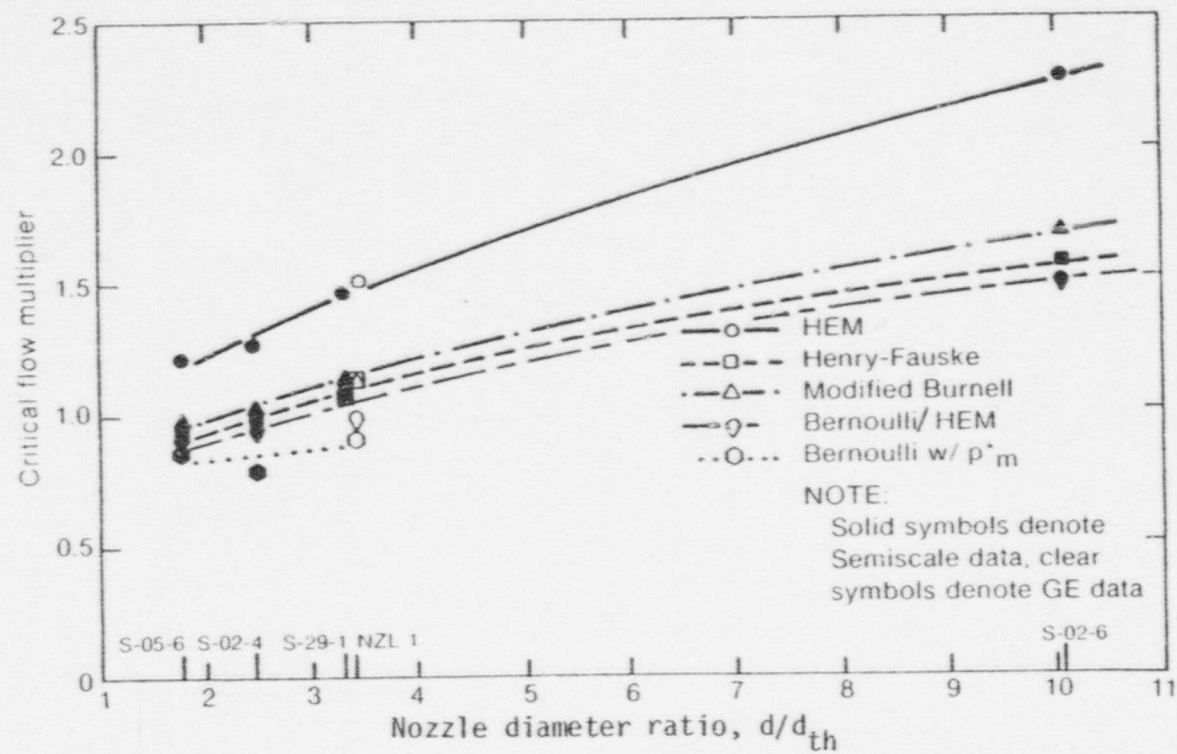


Fig. 7 Effect of nozzle diameter ratio on subcooled regime critical flow multipliers.

the throat area. This reduction in the effective flow area would have to be accounted for in the value of the critical flow multiplier since it is not accounted for analytically in the critical flow models and would result in the curves in Figure 7 exhibiting maximums.

The variation in the calculational accuracies which can be expected when using the critical flow multipliers presented in Figure 7 are presented in Figure 8 as a function of nozzle diameter ratio. The accuracies of the Henry-Fauske and Bernoulli/HEM models do not vary greatly with nozzle area ratio and are between ± 6 and $\pm 7\%$, respectively. Figure 8 shows that the Henry-Fauske model produced slightly more accurate results than the Bernoulli/HEM model, which is shown in Table III to be the best model to use in calculating critical flows in nozzle flow passages when the stagnation conditions are subcooled. The data presented in Table III are based upon all of the available data rather than just the data having stagnation universal qualities between zero and -0.5% . The data presented in Table III also shows that the Bernoulli/HEM RMS percent deviations are lower than the corresponding Henry-Fauske values for all nozzles except the smallest one (Semiscale Test S-02-6). The variations in the HEM and Modified Burnell critical flow multipliers in Figure 8 are well behaved at lower diameter ratios, but the values obtained using data from Semiscale Test S-02-6 ($d/d_{th} = 10.07$) do not seem to be consistent with the data at the lower diameter ratios. For this reason the HEM and Modified Burnell RMS percent deviations listed in Table III, which were calculated using all of the available data, have been added to the plot and an extension of the data presented at lower diameter ratios has been connected to these points. As was noted for the critical flow multipliers, the RMS percent deviations associated

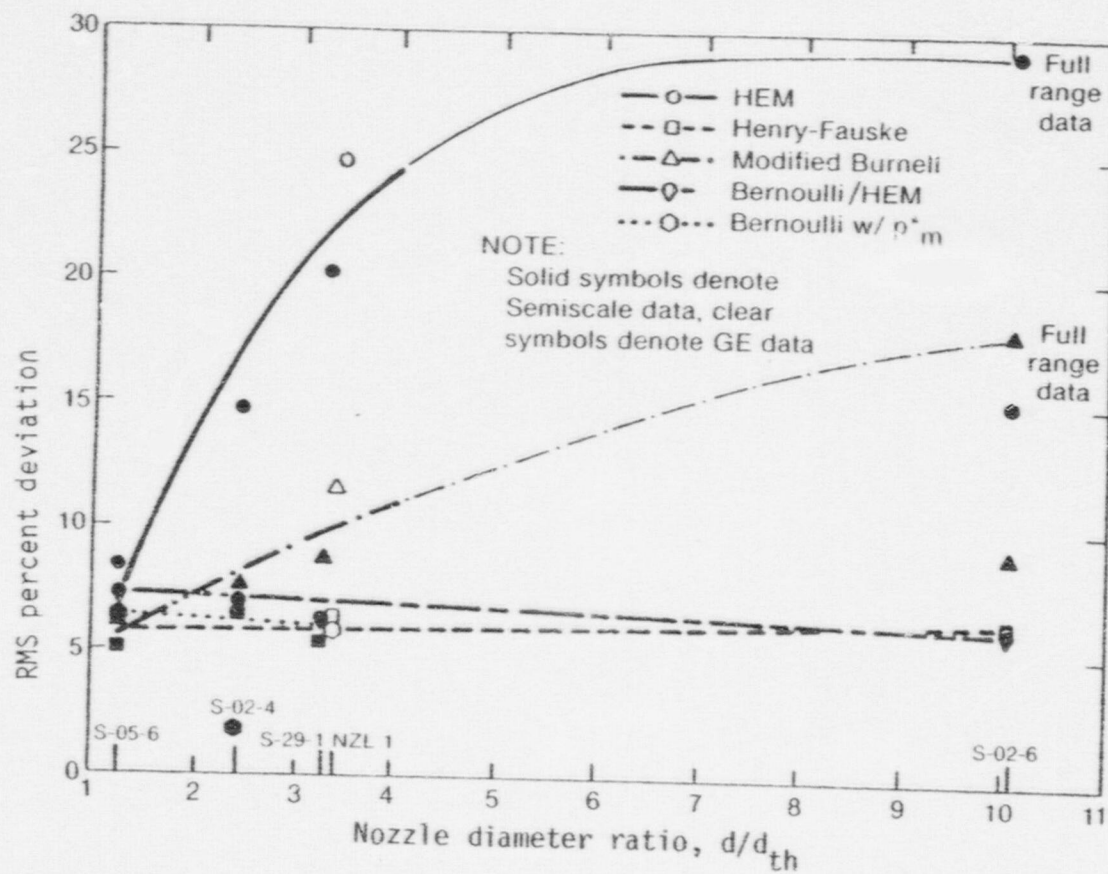


Fig. 8 Effect of nozzle diameter ratio on subcooled regime RMS percent deviations.

with Semiscale Test S-29-1 and GE Nozzle 1 are quite similar with the Henry-Fauske and Bernoulli/HEM values actually being in good agreement.

3.1.2 Transition Conditions. The variation with nozzle diameter ratio of the critical flow multipliers to be used when the stagnation conditions include qualities between zero and 2% is presented in Figure 9. No data were available for the transition quality regime for Semiscale Test S-02-6 and therefore information is available only for a very limited range of nozzle diameter ratios. All of the multipliers associated with the four critical flow models exhibit the need for progressively larger critical flow multiplier values as the diameter ratio increases. The multiplier values associated with the Bernoulli mass flux expression into which measured throat pressures were substituted for the critical pressure shows an asymptotic increase with increasing diameter ratio.

The calculational accuracy information presented in Figure 10 covers an even more restricted range of nozzle diameter ratios due to the lack of Semiscale Test S-02-6 data in the transition regime and the existence of only one data point in the transition quality regime for Test S-05-6. The Bernoulli/HEM model clearly is capable of the most accuracy for transition stagnation conditions. Calculational accuracies for stagnation conditions in the transition regime are the worst of those associated with the three quality regimes. This increase is probably a result of the changing nature of flow at stagnation conditions corresponding to the transition regime. The problems of modeling critical flows at very low stagnation qualities is discussed in Appendix A.

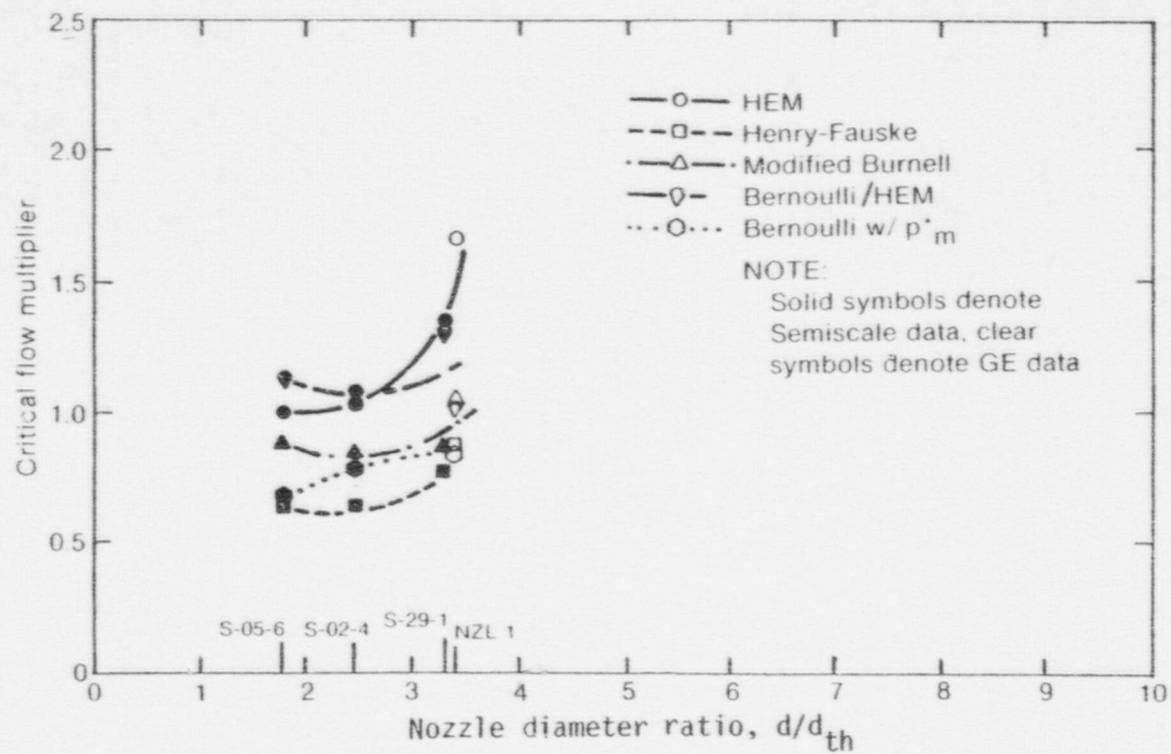


Fig. 9 Effect of nozzle diameter ratio on transition regime critical flow multipliers.

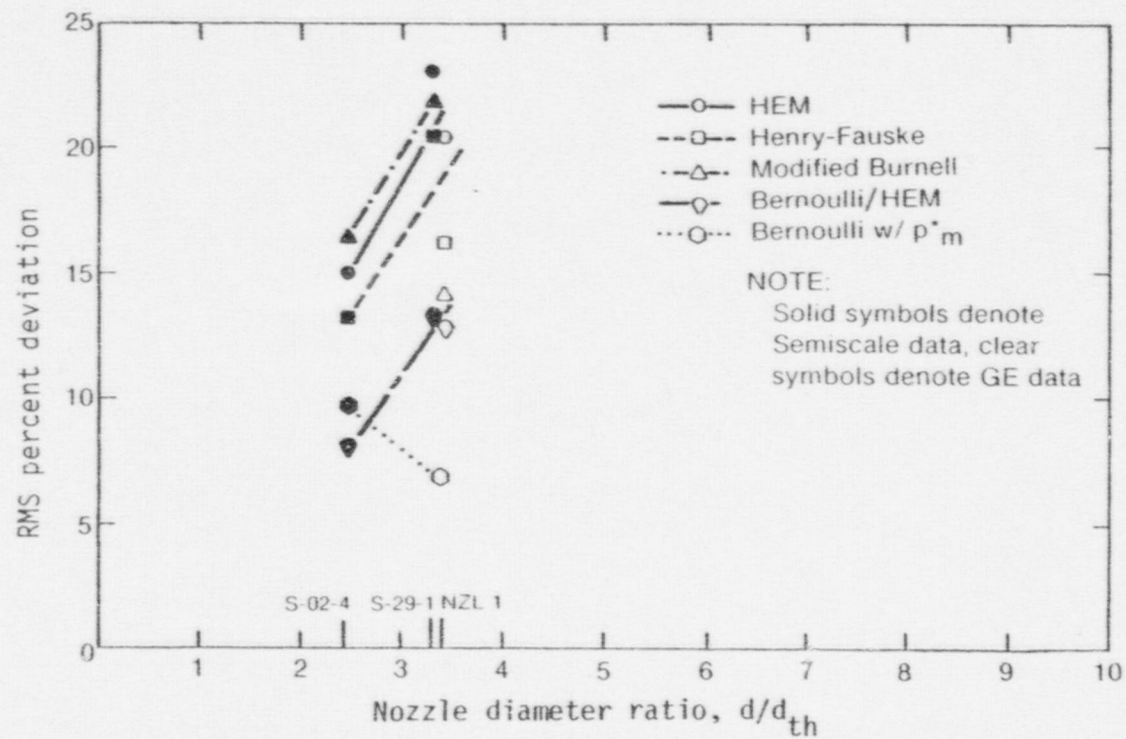


Fig. 10 Effect of nozzle diameter ratio on transition regime RMS percent deviations.

The critical flow multipliers and calculational accuracies associated with Semiscale Test S-29-1 and GE Nozzle 1 are shown to be in fair agreement in Figures 9 and 10.

3.1.3 Saturated Conditions. The variation in critical flow multiplier values for calculating critical flows when the stagnation conditions include qualities greater than 2% is presented in Figure 11 as a function of nozzle area ratio. The variation of the critical flow model multiplier values is well-behaved with the exception of the data associated with Semiscale Test S-05-6. These data appear to be consistently about 20% too high although checks made of the Test S-05-6 break flow measurements failed to show that the data was questionable. The existence of a minimum in the curves is not believed at this time and requires additional investigation.

The variation in calculational accuracy presented in Figure 12 shows that the homogeneous equilibrium model can be used to calculate critical flow rates to within ± 3 to $\pm 4\%$ occurring in nozzles having small diameter ratios. This accuracy degenerates to nearly $\pm 9\%$ at the largest diameter ratio for which data was available (Semiscale Test S-02-6). The Modified Burnell and Henry-Fauske model accuracies are well behaved functions of nozzle diameter ratio. These models provide better accuracy than HEM at the larger diameter ratios. The values presented for Semiscale Test S-29-1 ($d/d_{th} = 3.29$) are not believed to be true measures of calculational accuracy because some of the stagnation property data and the measured break flow rates contained a lot of noise^[a]. For this

[a] A discussion of the basic data is contained in Appendix A.

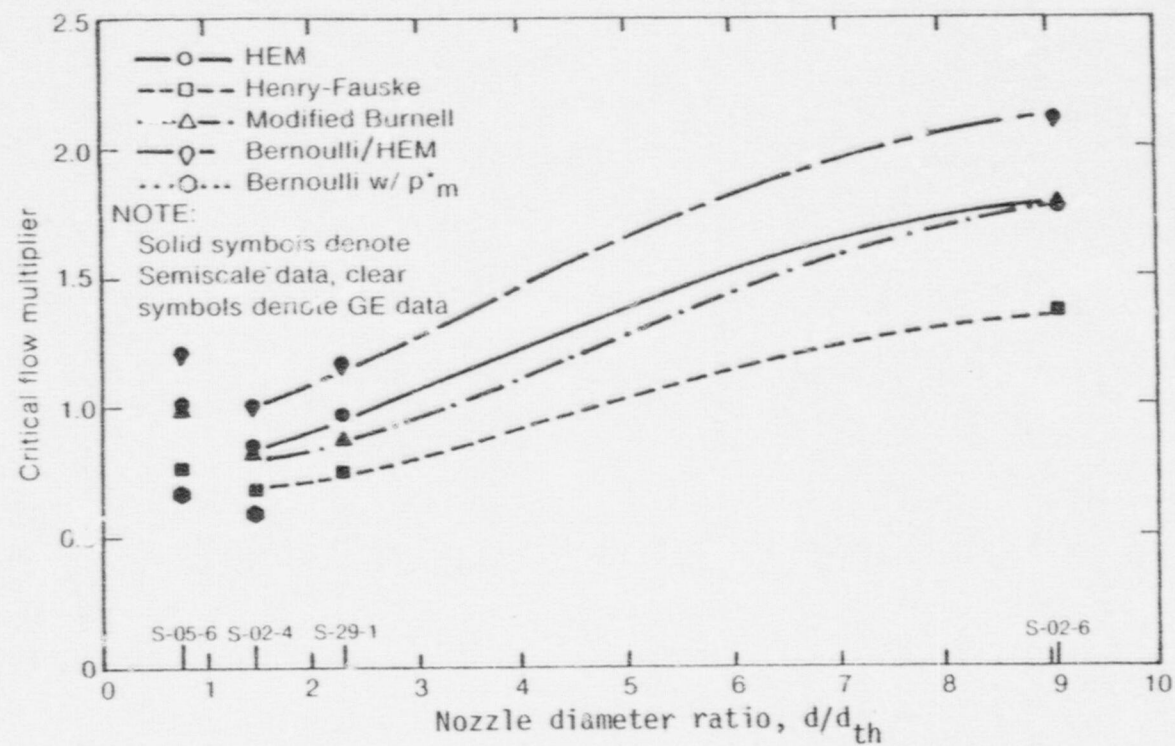


Fig. 11 Effect of nozzle diameter ratio on saturated regime critical flow multipliers.

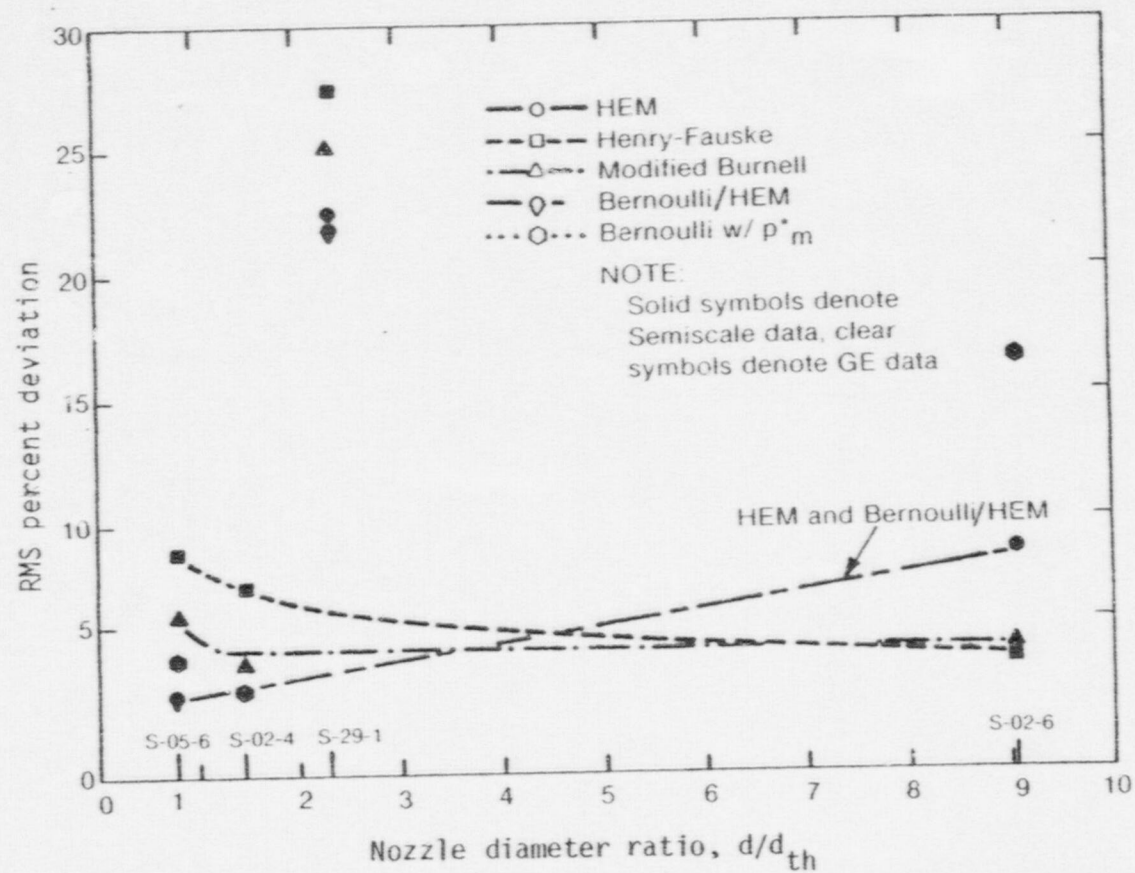


Fig. 12 Effect of nozzle diameter ratio on saturated regime RMS percent deviations.

reason the Test S-29-1 values are shown, but have been ignored in establishing the functional dependence of calculational accuracy on nozzle area ratio in Figure 12. The Bernoulli mass flux accuracy data is quite high at an diameter ratio of ten compared to the values at the smaller diameter ratios. This result is probably principally due to break flow inaccuracies suspected to have occurred in Semiscale Test S-02-6, but is also partially due to the assumption of incompressible flow incorporated in the model not being appropriate for conditions in which significant mass transfer can occur.

3.2 Tubular Flow Passages

Data for tubular flow passages, similar to that which have already been discussed for nozzle flow passages, are presented in this subsection. The majority of the data presented is from the General Electric tests, which did not include data at stagnation qualities greater than 2%. Therefore, the effect of length-to-diameter ratio on only subcooled and transition critical flow multipliers and associated calculational accuracies is discussed.

3.2.1 Subcooled Conditions. The effect of tube length-to-diameter ratio on value of subcooled multipliers is presented in Figure 13. All of the data presented in Figure 13, with the exception of that for Semiscale Test S-06-5, were calculated using data at stagnation universal qualities between zero and -0.2%. The Test S-06-5 values were calculated using data at stagnation universal qualities between zero and -0.5%. The data for all five of the analytical critical flow models exhibit the same trends. The scatter in the HEM data is notably large, but this is probably the

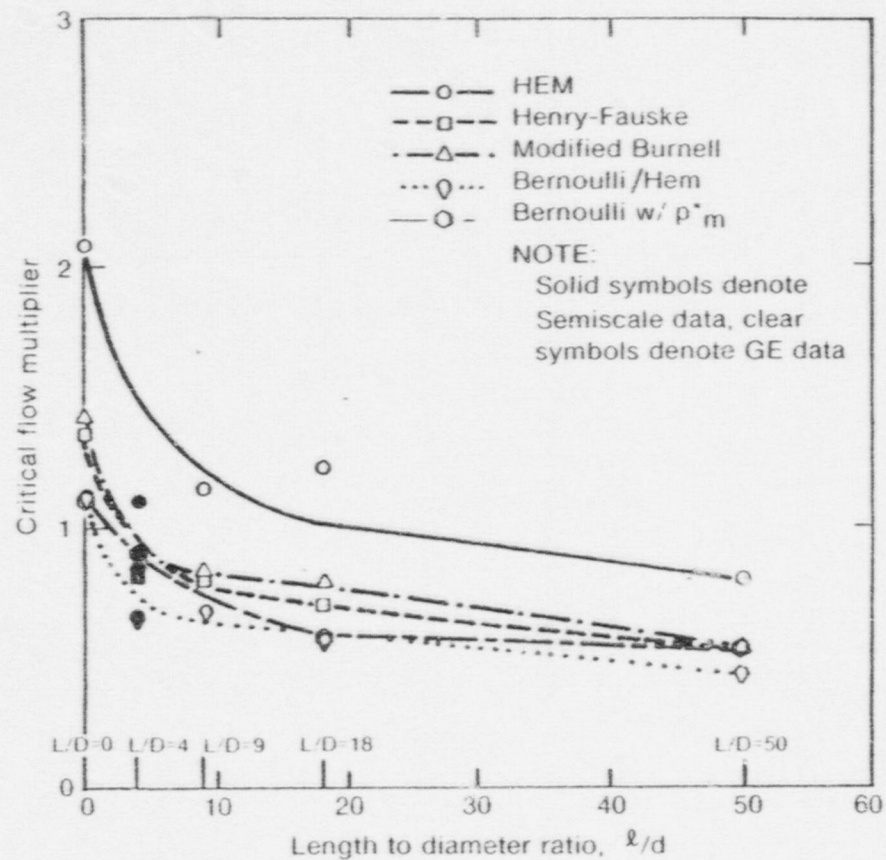


Fig. 13 Effect of tubular length-to-diameter ratio on subcooled regime critical flow multipliers.

result of the scarcity of data points. It is noteworthy that the data from Semiscale Test S-06-5 ($l/d = 4$) fit in well with the General Electric data. It is also interesting to note that the HEM critical flow multiplier attains a value of unity at an l/d of approximately eighteen or a length of approximately 23 centimeters for the 1.270 centimeter diameter tubes with which the data was generated, although the scatter in the data is notably large. This result is at variance with the results reported in Reference 11, which concluded, based on the same data and using the same criterion, that a length of only approximately thirteen centimeters was required to achieve equilibrium at the choke point and thus not require a critical flow multiplier.

Another facet of some of the data presented in Figure 13 which tends to support the conclusion reported in Reference 11 is that a knee occurs in the curves for the Henry-Fauske and Modified Burnell critical flow models and for the Bernoulli mass flux expression. The position of the knee is the dividing point between when nonequilibrium effects have a significant effect on the critical flow rate and when frictional pressure losses have a significant effect, the position of the knee can be used as an indicator of the length or l/d at which equilibrium is achieved at the choke point. The occurrence of knees in the curves at an l/d of approximately 9 or a length of approximately 11.5 centimeters is in good agreement with the tube length of approximately 13 centimeters or $l/d = 10$ required to achieve equilibrium at the choke point as concluded in Reference 11. A further discussion of the comparison of the results of the present study with those reported in Reference 11 is included in Appendix B.

The variation in RMS percent deviation with length-to-diameter ratio presented in Figure 14 contains anomalies which are attributable to the small number of available data points. The HEM data vary over a range from ± 3.5 to $\pm 14.5\%$. The HEM data at l/d 's = 0, = 9, and = 50 have been joined to define an upper bounding curve. The HEM data at l/d 's = 4 and = 18 have much lower values because these data were generated using data that covered only part of the stagnation universal quality range from zero to -0.2% . Therefore, these data do not reflect the full variation of the data over the quality range that was selected; consequently, they have lower RMS percent deviations. The Modified Burnell data are not well-behaved either because of the scarcity of data or the fact that the data is clustered and does not cover the quality range completely. The lack of agreement between the data for the $l/d = 50$ flow passage and the trends in the Henry-Fauske and Bernoulli/HEM data at lower values of l/d is probably associated with the fact that the calculations for the $l/d = 50$ case were made without accounting for viscous losses in the duct. Not accounting for viscous losses probably led to higher RMS percent deviations. The Henry-Fauske values are in Figure 14 to be most consistently the lowest which is why this model is recommended for calculating critical flows in tubular flow passages with subcooled stagnation conditions.

3.2.2 Transition Conditions. The data presented in Figure 15 show the variation in critical flow multipliers for use in calculating critical flow rates when the stagnation conditions include qualities between zero and 2% as functions of length-to-diameter ratio. The data is well behaved with an acceptable amount of scatter. The Semiscale

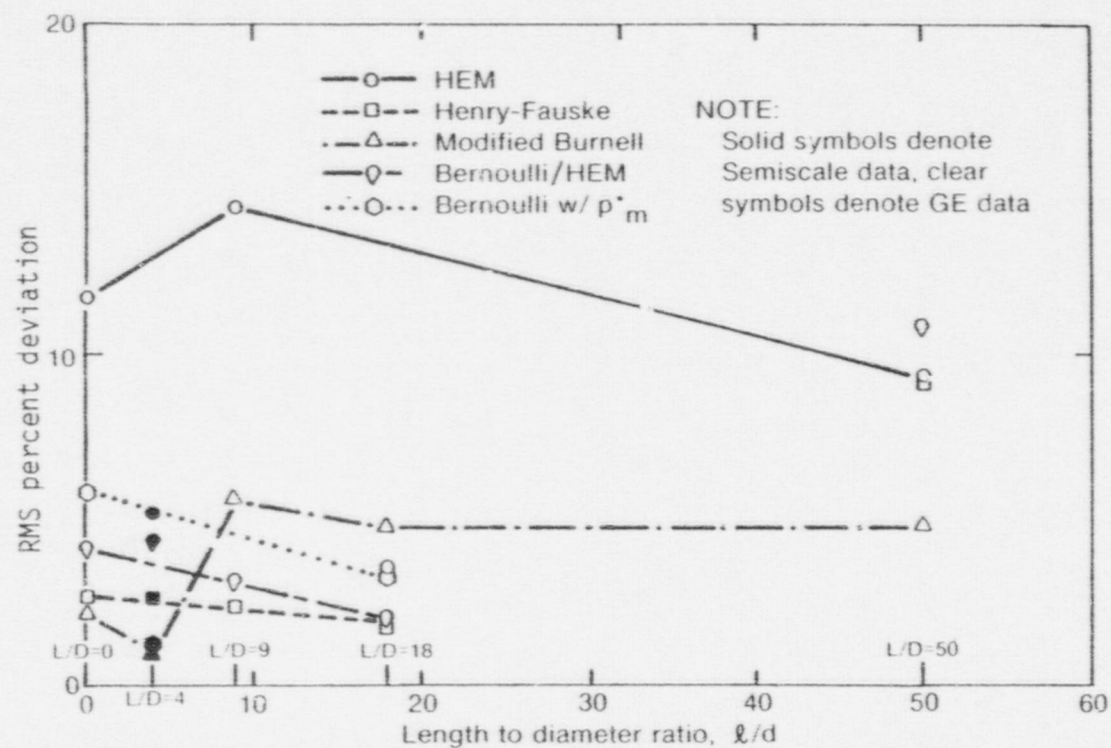


Fig. 14 Effect of tubular length-to-diameter ratio on subcooled regime RMS percent deviations.

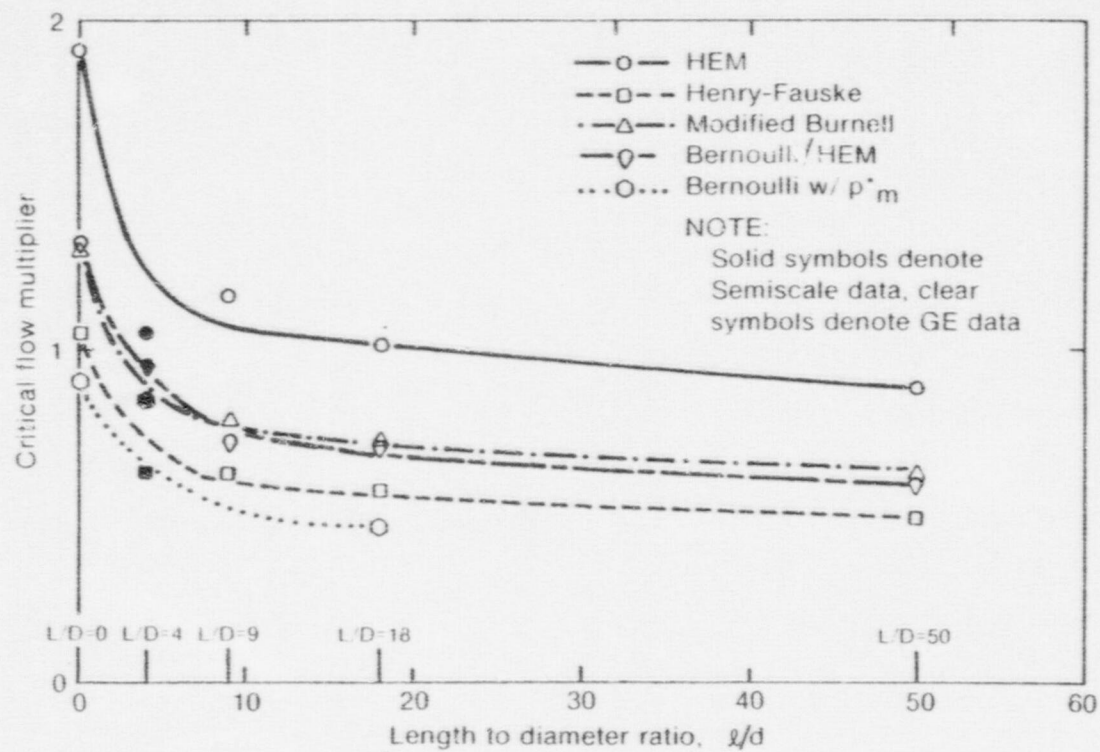


Fig. 15 Effect of tubular length-to-diameter ratio on transition regime critical flow multipliers.

Test S-06-5 data fits in well with the General Electric data. An l/d ratio of twenty ($l = 25$ centimeters) is shown to be required before the HEM critical flow multiplier assumes a value of unity, indicating that equilibrium conditions can be achieved at the choke point in a tube having this length-to-diameter ratio for stagnation qualities less than 2%. This result is at variance with the results reported in Reference 11. However, use of the knees in the Henry-Fauske, Modified Burnell, and Bernoulli mass flux expression serves as indicators of the l/d at which equilibrium is achieved at the choke point, results in excellent agreement between the results of this study and those reported in Reference 11.

The variation in RMS percent deviation presented in Figure 16 shows that the accuracy of the calculations become better with increasing length-to-diameter ratio except for the case of the Bernoulli/HEM model and the Bernoulli mass flux expression. In the case of the Bernoulli/HEM model, this result is probably due to the quality-weighted average technique with which critical flow rates are calculated at transition regime stagnation qualities. The Bernoulli mass flux expression RMS percent deviations at the smaller l/d 's are approximately equal to the lowest values achieved using the HEM, Henry-Fauske, and Modified Burnell models. The lack of data at larger l/d values makes it questionable whether the increasing trend exhibited by the Bernoulli data at low l/d 's would actually continue at higher l/d 's and result in RMS percent deviation values that were significantly larger than those of the three critical flow models.

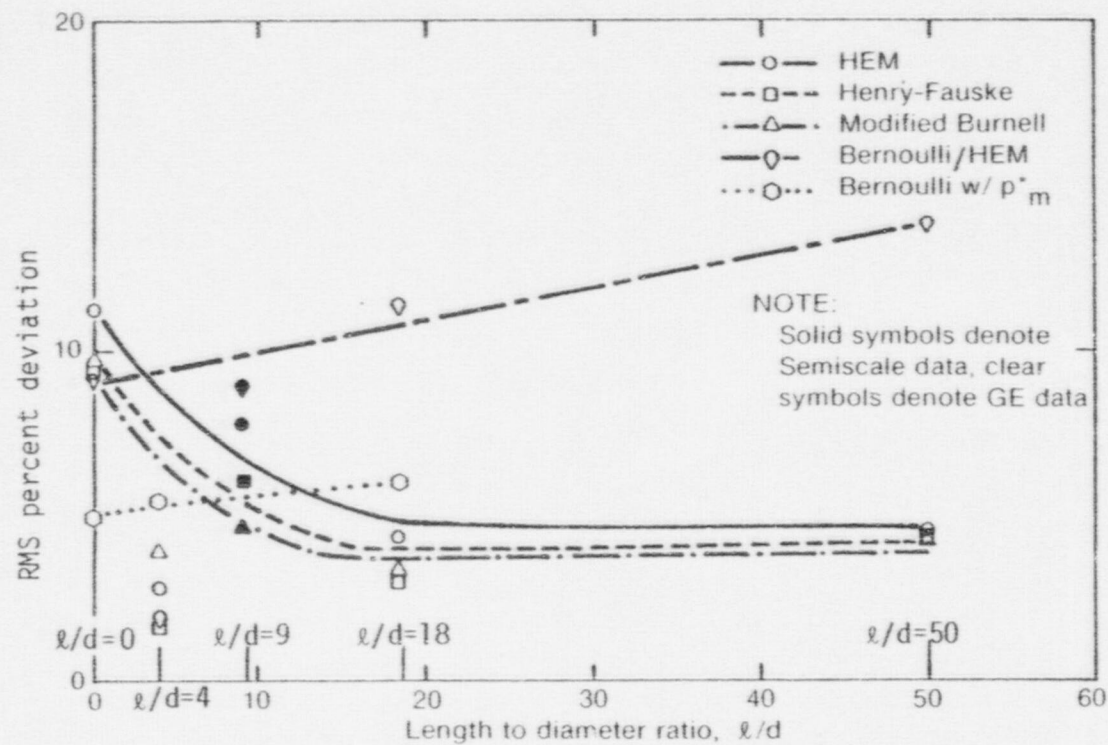


Fig. 16 Effect of tubular length-to-diameter ratio on transition regime RMS percent deviations.

The RMS percent deviations associated with the four critical flow models, which were calculated using data from Semiscale Test S-06-5, do not agree with the trends exhibited by the General Electric data. These discrepancies are thought to be the result of the greater quantity of data available from Test S-06-5 and the fact that the Semiscale data covers a range of stagnation qualities above the quality ranges covered by the General Electric data as shown in Table IV.

The RMS percent deviation data presented in Figure 16 and Table IV for tubes indicated that the accuracies of the Modified Burnell and Henry-Fauske models are similar for very low stagnation qualities. The Henry-Fauske values are lower than the Modified Burnell values for three out of the five configurations for which data was available and therefore the Henry-Fauske model is recommended for computing critical flows in tubular flow passages.

V. CONCLUSIONS AND RECOMMENDATIONS

A method for empirically determining critical flow multipliers and associated calculational accuracies for critical flow models has been developed. The method was applied to determine critical flow multipliers and calculational accuracies for experiments with five different nozzles, five different tubes, and an orifice. The Bernoulli/HEM best predicted the critical flow rates in the nozzles and orifice. The Henry-Fauske model performed best for tubes at subcooled and transition stagnation conditions, and the HEM demonstrated superior accuracy for the single tube tested at saturated stagnation qualities above 2%.

The effect of stagnation quality range spanned by the data is less than 0.1 variation in the critical flow multipliers for the recommended models. The critical flow rate data for the nozzles and tubes could be predicted within $\pm 10\%$ even if the critical flow multiplier was not based on data in the same range of stagnation qualities as the predictions. The Bernoulli/HEM and Henry-Fauske critical flow multipliers and calculational accuracies for nozzles and tubes, respectively, are reasonably well behaved functions of nondimensional geometric parameters.

Of the critical flow models currently available in RELAP4, the Henry-Fauske/HEM combination critical flow model is the best for general purpose application. This selection is based on the overall comparisons of the individual models to all tests, and does not include any comparisons in the transition regime. Better calculational accuracies may be achieved

by using the information presented in Tables III, IV, and V to select an appropriate critical flow model for a specific flow situation.

The general conclusion of the study is that good predictions of critical flow rates in specific nozzles, tubes, and orifices can be achieved with current analytical models. The critical flow multipliers and calculational accuracies presented in Tables III and IV permit the prediction of critical flows in nozzles and tubes with known accuracy when the fluid stagnation conditions are known. However, the range of fluid conditions and size of flow passages for which the information in Tables III, IV, and V is valid must be investigated in a subsequent study. For integral system calculations, the uncertainty of the critical flow rate predictions cannot be completely determined from the reported calculational accuracies; the uncertainty of the system model critical flow rate calculation depends in part on the accuracy with which the stagnation conditions (critical flow model input) can be predicted. Finally, scale effects have not been fully addressed and may result in a significant bias type error in the critical flow multiplier.

This report identified areas in which additional work could strengthen the results. The results should be applied to additional data with a wider range of fluid conditions and a variety of flow passage geometries and scale to verify the predictability and accuracy of calculated flows. The data can be refined in several ways, such as mathematically filtering to remove random errors and removing the time weighting as discussed in Appendix B. Multipliers and accuracies for tubular flow passages could

be derived by an iterative procedure which would account for viscous losses in the duct. Critical flow multipliers thus derived would not have to account for viscous losses and would be less sensitive to variations in the range of stagnation conditions. Transition qualities could be analytically determined to optimize both transition and saturated critical flow predictions.

Areas of investigation not specifically related to the data generated in the course of the study were also identified. Information about critical flows in tubes was not available at stagnation qualities greater than 1% except for Semiscale Test S-06-5 (tube $L/d = 4$). A data base should be assembled for flow through tubes at higher stagnation qualities. The Bernoulli mass flux expression is capable of producing superior comparisons to measured critical flow rates at subcooled and transition stagnation conditions in nozzles and orifices. A correlation should be derived for critical pressures in nonequilibrium critical flow. The correlation could then be used in conjunction with the Bernoulli mass flux expression for improved predictions of critical flow rates.

The Bernoulli/HEM should be included as a critical flow model option in the RELAP4 code because of the good predictive capabilities exhibited in this study. The temperature dependence of the critical pressure ratio function should be investigated. The method of computing critical flow rates at transition qualities with the Bernoulli/HEM could probably be improved; the quality weighted averaging technique currently employed does not have any physical significance.

A data base should be assembled to address the question of scaling parameters for critical flow. Diverse opinions have been expressed in the technical literature supporting either absolute length or diameter as opposed to nondimensional parameters. Scaling of critical flow calculations must be resolved for system model calculations of postulated full scale loss-of-coolant accidents.

Continued investigations in all areas of critical flow modeling depend on having a critical flow data base covering a wide range of flow geometries and fluid conditions. A centralized critical flow data bank should be established to provide readily accessible, uniformly formatted data. In order to be of maximum use, critical flow data should include corresponding stagnation state data, critical flow rate data, and if possible critical state (at least critical pressure) data.

VI. REFERENCES

1. D. G. Hall, A Study of Critical Flow Prediction for Semiscale Mod-1 Loss-of-Coolant-Accident Experiments, TREE-NUREG-1006 (December 1976).
2. K. R. Katsma, et al., RELAP4/MOD5 A Computer Program for Transient Thermal-Hydraulic Analysis of Nuclear Reactor and Related Systems, ANCR NUREG-1335 (September 1976).
3. R. F. Henry and H. F. Fauske, The Two-Phase Critical Flow of Two-Component Mixtures in Nozzles, Orifices, and Short Tubes, Journal of Heat Transfer, (May 1971) pp. 179-187.
4. J. W. Burnell, "Flow of Boiling Water Through Nozzles, Orifices, and Pipes," Engineering, (December 1947) pp. 572-576.
5. L. S. Tong, Boiling Heat Transfer and Two Phase Flow, New York: John Willey and Sons, Inc. 1965, pp. 108-110.
6. E. M. Feldman and K. E. Sackett, Experiment Data Report for Semiscale Mod-1 Tests S-05-6 and S-05-7 (Alternate ECC Injection Tests), TREE-NUREG-1055 (June 1977).
7. H. S. Crapo, M. F. Jensen, and K. E. Sackett, Experiment Data Report for Semiscale Mod-1 Test S-02-4 (Blowdown Heat Transfer Test), ANCR-1234 (November 1975).

8. H. S. Crapo, M. F. Jensen, and K. E. Sackett, Experiment Data Report for Semiscale Mod-1 Test S-29-1 (Integral Test with Asymmetrical Break), ANCR-NUREG 1327 (July 1976).
9. B. L. Collins, H. S. Crapo, and K. E. Sackett, Experiment Data Report for Semiscale Mod-1 Test S-02-6 (Blowdown Heat Transfer Test), TREE-NUREG-1037 (January 1977).
10. V. Esparza and K. E. Sackett, Experiment Data Report for Semiscale Mod-1 Test S-06-5 (LOFT Counterpart Test), TREE-NUREG-1125 (June 1977).
11. G. L. Sozzi and W. A. Sutherland, Critical Flow of Saturated and Subcooled Water at High Pressure, NEDO-13418 (July 1975).

Appendices A and B are on microfiche.